

**OXIRED 02  
– Work Package 3 –**

---

**Reactive Transport  
Modeling**

---

**Report on Task 3.4**

submitted to

**KOMPETENZZENTRUM**  
WasserBerlin

by

UIT GmbH Dresden  
Zum Windkanal 21, D-01109 Dresden, Germany

Project financed by:



---

**Dresden, Mar 2011**



## DELIVERABLE D 3.4

---

# Reactive Transport Modeling of TUB Column Tests

---

AUTHORS: Dr. Harald Kalka  
Dr. Jana Nicolai



**UMWELTLEISTUNGEN**

CONTACT: Dr. Harald Kalka  
Phone: +49-351-8 86 46 40  
Fax: +49-351-8 86 57 73  
E-Mail: [h.kalka@uit-gmbh.de](mailto:h.kalka@uit-gmbh.de)

PROJECT PARTNER: Technische Universität Berlin

Dr. Traugott Scheytt  
Dr. Dirk Radny  
Beate Müller





# CONTENTS

1	INTRODUCTION.....	5
1.1	Background and Objectives.....	5
1.2	The Model .....	6
1.3	List of Abbreviations.....	7
2	EXPERIMENTAL SETUP AND MODEL INPUT .....	9
2.1	Experimental Setup .....	9
2.2	Model Configuration and Input Parameters .....	11
2.2.1	Geometry & Hydraulics .....	11
2.2.2	Two-Layer Model .....	13
2.2.3	Aqueous Solutions .....	14
2.2.4	Thermodynamic Database.....	15
3	HYDRAULICS AND HYDROCHEMISTRY .....	17
3.1	Advection and Dispersion .....	17
3.2	Cation Exchange.....	18
3.3	Mineral Phases .....	22
3.3.1	Theoretical Background .....	22
3.3.2	Model Calculations .....	23
3.3.3	Comparison of three Calcite-Precipitation Models.....	26
4	REDOX REACTIONS .....	27
4.1	Theoretical Background .....	27
4.2	Experimental Evidence for Redox Reactions.....	29
4.3	Redox Sequences in the Column Tests .....	30
4.4	Biodegradation and Enzyme Kinetics .....	31
4.4.1	Conceptual Model .....	31
4.4.2	Model Parameters and Initial Conditions.....	34
4.5	Application and Model Results .....	37
4.5.1	Model Calculations versus Experiments.....	37
4.5.2	Interpretation – Redox Zonation inside Columns .....	41
4.5.3	Limits and Benefits .....	43
5	SUMMARY .....	45
	REFERENCES.....	47

## APPENDIX..... 49

A	REACTIVE TRANSPORT .....	51
A.1	Definition of the System.....	51
A.1.1	Aqueous and Mineral Phases .....	51
A.1.2	Main Equations .....	52
A.2	Transport Phenomena.....	53
A.2.1	Advection in a Homogeneous System.....	53
A.2.2	Advection in a Heterogeneous System.....	54
A.2.3	Dispersion .....	55
A.2.4	Numerical Model versus Analytical Solution .....	57



A.3	The Software.....	59
B	ENZYME KINETICS .....	61
B.1	Michaelis-Menten Equation .....	61
B.2	Enzyme Inhibition – HALDANE Equation.....	63
B.3	Microbial Growth Dynamics – MONOD Kinetics.....	65

# 1 INTRODUCTION

## 1.1 Background and Objectives

The project OXIRE2 started in January 2010 as a continuation of OXIRE1. The project is guided by KompetenzZentrum Wasser Berlin (project leader Dr. G. Grützma-cher); it is sponsored by Berliner Wasserbetriebe (BWB) and VEOLIA Eau.

OXIRE2 comprises three Work Packages:

- |      |  |
|------|--|
| WP 1 | Laboratory, Technical, and Pilot Scale Experiments<br>(by TUB, UBA, and KWB) |
| WP 2 | Selection and Preparation of Demonstration Site<br>(by KWB)                  |
| WP 3 | Redox Control and Optimization at AR Ponds<br>(by TUB and UIT)               |

WP3 consists of two main parts and was performed in cooperation with TUB:

- |         |   |
|---------|---|
| Part I. | Laboratory column experiments with special emphasis on sedi-ment characteristics (by TUB) |
| Part II | Numerical modeling of the results of the TUB column experi-ments (by UIT)                 |

The present report belongs to Part II of WP3.

**Motivation.** In Berlin, around 70 % of abstracted groundwater originates from river-bank filtration and artificial recharge (AR). A description of AR is given in [KWB10]. Fig. 1.1 shows a typical AR system which contains four elements: infiltration pond, hy-porheic zone, subsurface passage, and production well.

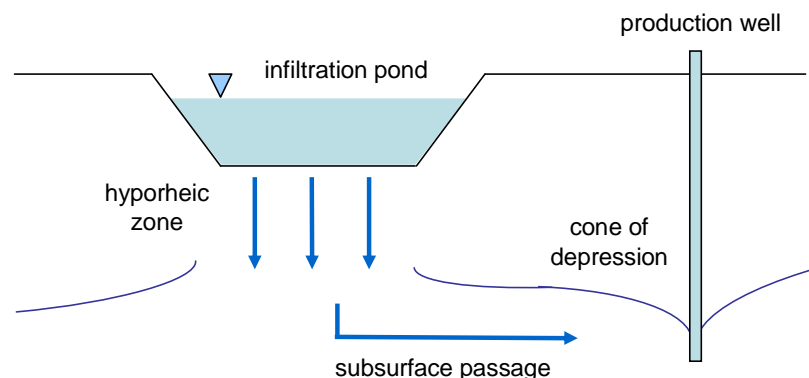


**Fig. 1.1** Artificial recharge system – AR (redrawn from [KWB10])

During percolation and subsurface passage the quality of the infiltrated water improves due to physical filtration, sorption and biodegradation. Biodegradation is a major driver for *redox zonation* and so it is highly influenced by redox conditions, too. The main purpose of WP3 is to investigate these processes in column experiments including its numerical simulation.

## 1.2 The Model

The column tests are simulated with the Reactive Transport Model TRN, version 1.7. TRN belongs to a well-tested family of other environmental models developed by UIT in the last 14 years. It is written in the object oriented language C++ using special chemistry classes which include the numerical routines of the USGS computer code PHREEQC [PA99]. A brief model description is given in Appendix A.

The model combines transport with geochemistry (thermodynamics *and* kinetics) and consists of three main parts as it is shown in Fig. 1.2:

- transport module (advection & dispersion; single and dual porosity)
- geochemical module (based on PHREEQC routines, thermodynamic databases, and kinetic models including enzyme kinetics)
- Graphical User Interface – GUI (data input, visualization, and scenario comparisons)

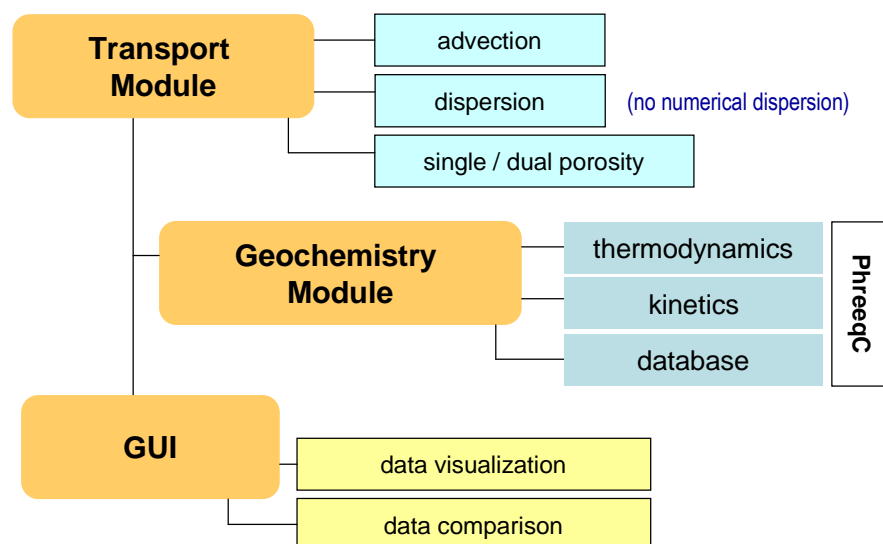


**Fig. 1.2** Modular structure of the Reactive Transport Model TRN

TRN is user-friendly and it is equipped with online graphics and data visualization tools. The user is able to interact with the running system and to check intermediate results. About 20 % of the source code deals with plausibility tests. In particular, at every time step TRN checks the local and global mass balance (in each cell and in the whole column). Any inconsistency generates an error message.

Adopting the ideas of [AP05] the transport model is free of *numerical dispersion*. This is a great advantage: fronts move neatly and remain sharp; they are only influenced by hydrodynamic dispersion.

A typical setup for 1D reactive transport is sketched in Fig. 1.3. The column (or flow path in the subsurface) is split into N cells. Each cell can be configured separately composing a flow path through different layers/zones.

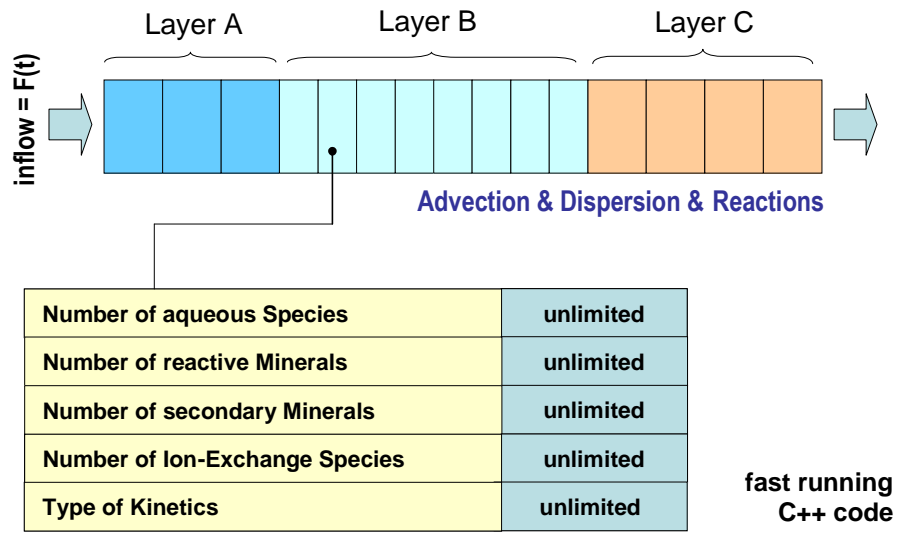


Fig. 1.3 Cell structure of 1D reactive transport column

### 1.3 List of Abbreviations

<b>ADR</b>	Advection-Dispersion-Reaction Equation
<b>AR</b>	Aquifer Recharge
<b>ATP</b>	Adenosine Triphosphate
<b>BF</b>	Bank Filtration
<b>BOD</b>	Biochemical Oxygen Demand
<b>BOM</b>	Bulk Organic Matter
<b>BWB</b>	Berliner Wasserbetriebe
<b>CBZ</b>	Carbamazepine
<b>CEC</b>	Cation Exchange Capacity
<b>COD</b>	Chemical Oxygen Demand
<b>DIC</b>	Dissolved Inorganic Carbon
<b>DO</b>	Dissolved Oxygen
<b>DOC</b>	Dissolved Organic Carbon
<b>DOM</b>	Dissolved Organic Matter
<b>DON</b>	Dissolved Organic Nitrogen
<b>EC</b>	Electrical Conductivity
<b>Eh</b>	Redox Potential in mV (relative to SHE)
<b>GUI</b>	Graphical User Interface



<b>GW</b>	Groundwater (also abbreviated by 'gw')
<b>HFO</b>	Hydrous Ferric Oxides
<b>IAP</b>	Ion Activity Product
<b>I/O</b>	Input/Output
<b>IT</b>	Information Technology
<b>IX</b>	Ion Exchange
<b>KWB</b>	KompetenzZentrum Berlin
<b>l.h.s</b>	left hand side (of an equation)
<b>LT</b>	Lake Tegel
<b>M</b>	Mol per Liter (concentration unit: 1 M = 1 mol/L)
<b>mM</b>	Millimol per Liter (concentration unit: 1 mM = 1 mmol/L)
<b>na</b>	not analyzed
<b>NA</b>	Natural Attenuation
<b>OC</b>	Organic Carbon
<b>ODE</b>	Ordinary Differential Equation
<b>ORP</b>	Oxidation-Reduction Potential (in short: redox potential)
<b>PDE</b>	Partial Differential Equation
<b>PhAC</b>	Pharmaceutically Active Compound
<b>POC</b>	Particular Organic Carbon
<b>POM</b>	Particular Organic Matter
<b>PON</b>	Particular Organic Nitrogen
<b>r.h.s</b>	right hand side (of an equation)
<b>RMS</b>	Root Mean Square (square root of variance)
<b>SHE</b>	Standard Hydrogen Electrode
<b>SI</b>	Saturation Index
<b>SMX</b>	Sulfamethoxazole
<b>TRN</b>	Reactive Transport Model developed by UIT and applied in this report
<b>TSS</b>	Total Suspended Solids
<b>TUB</b>	Technische Universität Berlin
<b>UBA</b>	Umweltbundesamt
<b>UIT</b>	Umwelt- und Ingenieurtechnik GmbH Dresden, Germany
<b>USGS</b>	U.S. Geological Survey
<b>XRD</b>	X-ray Diffraction
<b>WP</b>	Work Package
<b>1D</b>	One Dimensional
<b>2D</b>	Two Dimensional
<b>3D</b>	Three Dimensional

## 2 EXPERIMENTAL SETUP AND MODEL INPUT

### 2.1 Experimental Setup

The column tests are performed at TU Berlin [TUB10]. Fig. 2.1 shows the experimental setup that consists of:

- closed container for the water
- upward flow through the column; flow velocities  $\sim 0.1$  to  $1$  m/d
- column is 35 cm in length, diameter of  $d = 13.5$  cm
- continuously measurement of pH, T, ORP, DO, EC at the outflow of the column
- eluted liquid was collected and sampled (one sample per hour with subsequent analysis of main cations and anions)

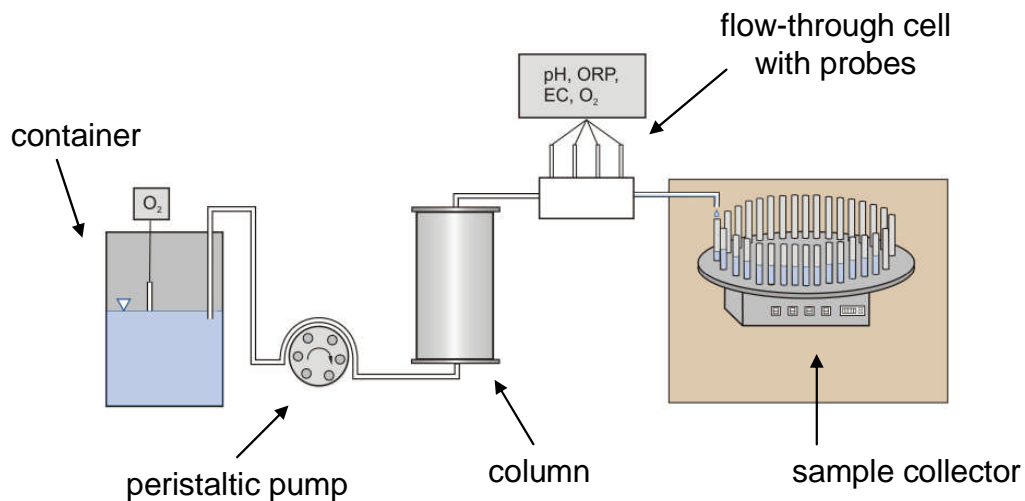


Fig. 2.1 Experimental setup of column tests (redrawn from [TUB10]).

In total, five column tests are performed at TUB. As shown in Tab. 2.1, the experiments differ by the pre-treatment of the sediment (not treated, treated at  $200^\circ\text{C}$  and at  $550^\circ\text{C}$ ) and by addition of iron coated sand. In this way, Col 1, Col 2, and Col 3 are mono-layer experiments, whereas Col 4 and Col 5 represent 2-layer experiments.

Tab. 2.1 Five column tests performed at TUB.

column	sediment	iron coated sand
1	not treated	no
2	not treated	no
3	24 h at $200^\circ\text{C}$	no
4	24 h at $200^\circ\text{C}$	10 cm at column exit (within anaerobic zone)
5	8 h at $550^\circ\text{C}$	10 cm at column entry (within aerobic zone)

**Inflow Water.** The inflow water for the column tests was taken from Lake Tegel (after micro-sieving). Its chemical composition is listed in Tab. 2.2 (only main parameters).

**Tab. 2.2** Inflow water composition (ozonated) taken from Lake Tegel.

inflow water		raw data
pH	-	8.0
ORP	mV	345
EC	$\mu\text{S/cm}$	940
Ca	mg/L	87.3
SO <sub>4</sub>	mg/L	93.5
NO <sub>3</sub>	mg/L	6.2
O <sub>2</sub>	mg/L	21.0
DOC	mg/L	7.9

Each column test takes about 14 days and comprises three phases (LT – Lake Tegel):

- Starting phase:
  - Influent: LT-water (not ozonated)
  - Duration of starting phase ~ 3 days
- Main phase:
  - Change of influent: LT-water (not ozonated) to LT-water (ozonated) after 10-12 days
  - Addition of a tracer
- Final phase:
  - Change of influent: LT-water (ozonated) to LT-water (not ozonated)

**Sediment.** The sediment was taken from infiltration pond Lake Tegel, Berlin, at a depth between 0 and 0.5 m below surface level. Typical sediment parameters are:

- Medium grain size: 0.38 mm
- Hydraulic conductivity (HAZEN):  $5.6 \cdot 10^{-4}$  m/s

The organic carbon content  $f_{\text{OC}}$  and the total carbon content  $f_{\text{C}}$  is listed in Tab. 2.1.

**Tab. 2.3** Organic carbon and total carbon content in soil samples of Col 2 to Col 5.

column	sediment	$f_{\text{OC}}$ [kg <sub>OC</sub> /kg <sub>soil</sub> ]	$f_{\text{C}}$ [kg <sub>C</sub> /kg <sub>soil</sub> ]
2	not treated	0.0017	
3	before column test	0.0017	
3	after column test, column entry	0.0016	
4	24 h at 200°C	0.0019	0.0022
5	8 h at 550°C	0.0006	0.0007

## 2.2 Model Configuration and Input Parameters

In total, five column tests (Col 1, Col 2, Col 3, Col 4, and Col 5) are performed by TUB, whereas Col 1 was run to test the experimental setup and it is not used in the numerical simulations. Col 2 was used to adjust the hydraulic parameters and CEC. A schematic overview of all column tests is given in Fig. 2.2.

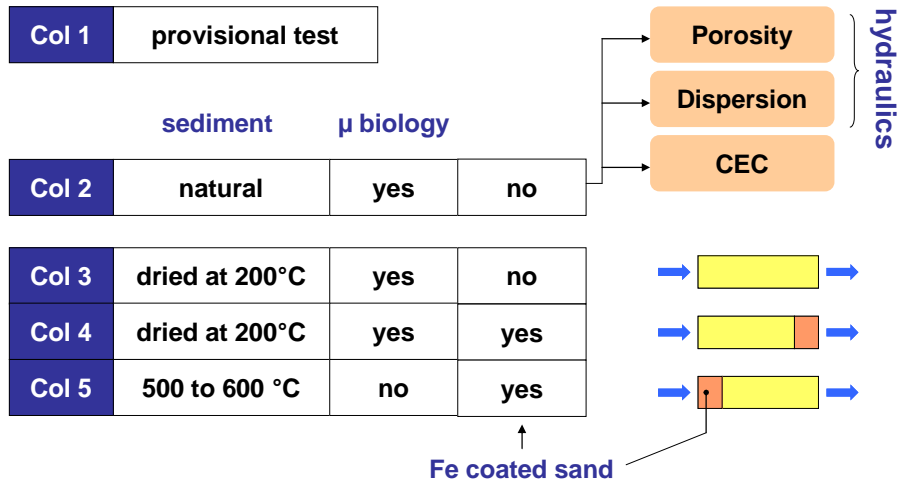


Fig. 2.2 Overview of the five column tests

### 2.2.1 Geometry & Hydraulics

**Geometry.** The geometry of the column is defined by:

total column length	$L = 35 \text{ cm}$
column diameter	$d = 13.5 \text{ cm}$
cross section	$A = \pi d^2/4 = 143 \text{ cm}^2$
total volume	$V = A \cdot L = 5.010 \text{ L}$
number of cells	$N = 35$
cell length	$\Delta x = L/N = 1 \text{ cm}$
porosity (of quartz sand)	$\varepsilon = 0.35$
total pore volume	$V_p = \varepsilon \cdot V = 1.753 \text{ L}$
pore volume of one cell	$\Delta V_p = V_p/N = 50.1 \text{ mL}$

**Hydraulics.** In the homogeneous system all cells have the same pore volume

$$(2.1) \quad \Delta V_p = \varepsilon A \cdot \Delta x$$

Given the volumetric flow  $Q$  as the constant inflow rate (pumping rate), the timestep width can be determined by

$$(2.2) \quad \Delta t = \frac{\Delta V_p}{Q} = \frac{\varepsilon A \Delta x}{Q}$$

The timestep  $\Delta t$  enters the model as a key input parameter (together with  $\Delta x$ ). The relation between *pore velocity*  $v$  and inflow rate  $Q$  is given as

$$(2.3) \quad v = \frac{Q}{\varepsilon A} = \frac{\Delta x}{\Delta t}$$

The pore volume is exchanged once completely after the time

$$(2.4) \quad T_p = \frac{V_p}{Q} = \frac{L}{v}$$

In the experiments the pumping rate was kept constant at approximately  $Q = 1$  mL/min; it varies slightly from column to column. The hydraulic parameters are listed in Tab. 2.4. The pore volume exchange  $T_p$  is in the range of one day.

**Tab. 2.4** Hydraulic parameters.

			Col 2	Col 3	Col 4	Col 5
inflow rate	Q	mL/min	1.3	1.3	1.0	1.1
pore velocity	v	cm/h	1.56	1.56	1.20	1.32
timestep	$\Delta t$	h	0.641	0.641	0.833	0.758
one pore exchange	$T_p$	h	22.4	22.4	29.2	26.5
duration of test	$T_{\text{test}}$	days	14	11	19	13

**Numerical Dispersion.** Using Eq. (2.3), i.e. the relationship  $\Delta t = \Delta x/v$  between time and distance discretization, numerical dispersion is minimized to zero [AP05]. This is a great advantage of the applied procedure. Thus, in case of pure advection we simply move along, pouring at every time step concentrations from one cell into the next one. Fronts move neatly and remain sharp (see, for example, blue curve in Fig. 3.2). Such sharpness is blurred when front transfer and grid boundaries do not correspond (i.e. when  $\Delta t \neq \Delta x/v$ ). In this case the mixing of old and new concentrations in a cell leads to gradual smoothing of transitions (which is called *numerical* dispersion). In conclusion, applying rigorously Eq. (A.24) the model becomes free of numerical dispersion. (A quite similar approach is used in the advection procedure of PHREEQC [PA99].)

The *hydrodynamic* dispersion was adjusted to the bromide breakthrough (see Fig. 3.2).

**Single vs. Dual Porosity.** The reactive transport model TRN allows the application of two principal concepts: single-porosity and dual-porosity. The *dual* porosity approach reflects the fact that in porous media pores are partly active (mobile) and partly inactive (immobile or stagnant). The inactive pores are filled with solution but the velocity inside those pores is negligible compared with the velocity in active pores. Thus, transport of dissolved solids is considered by advection and dispersion in active (mobile) pores while the diffusion process dominates in the stagnant pores. The interplay between mobile and stagnant pores is often described by a first-order mass transfer  $\alpha$  ( $\alpha$  enters Eqs. (A.6) and (A.7), respectively).

However, in order to keep the present model simple all calculations are performed in the *single*-porosity approach (rather the dual-porosity model). This is supported by the data itself where the bromide peak (tracer) is almost symmetric. In this way we do not need the extra mass-exchange parameter  $\alpha$  (which is unknown and requires additional effort to be adjusted).

### 2.2.2 Two-Layer Model

Col 1, Col 2, and Col 3 represent a homogenous system (mono-layer). In addition to these experiments, Col 4 and Col 5 contain one layer of iron-coated sand (of 10 cm thickness). As shown in Fig. 2.3, two configurations of the two-layer system are considered: Fe-coated sand at the column entry (Col 4) and Fe-coated sand at the column exit (Col 5). The porosity of Fe-coated sand is assumed to be equal to that of pure sand, i.e. the flow velocity in the two-layer model does not change.

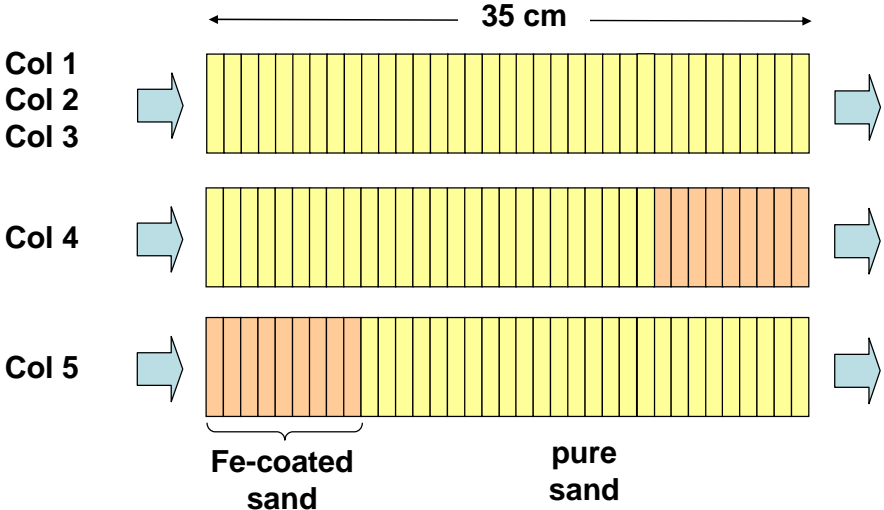


Fig. 2.3 Column setup with 35 cells as a mono-layer and two-layer system.

The Fe-coated sand should enhance the adsorption capacity of the sediment (due to HFO phases) and retard inorganic and organic contaminants. The longer residence time within this zone would provide more time for biodegradation.

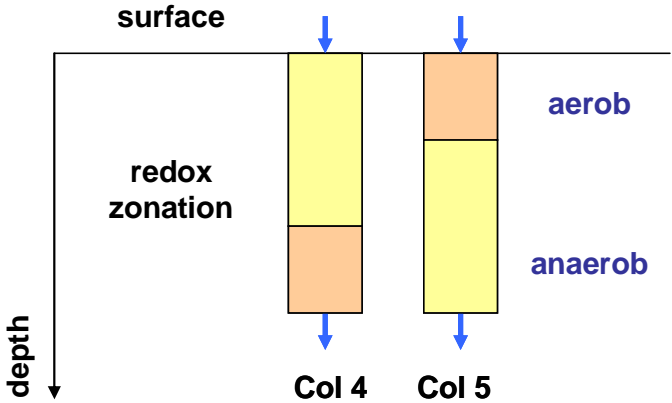


Fig. 2.4 Column setup and redox zonation

The location of the iron-coated sand, once at the column exit and once at the column entry should mimic anaerobic degradation (Col 4) and aerobic degradation (Col 5). The idea behind this column design is illustrated in Fig. 2.4 where water percolates through the subsurface and passes different redox zones.

### 2.2.3 Aqueous Solutions

The *geochemical* input comprises several aspects:

- the aqueous solutions for both *inflow* and *initial* waters
- the ion exchanger see § 3.2
- the equilibrium minerals see § 3.3

as well as

- thermodynamic database see § 2.2.4
- kinetic parameters for calcite see § 3.3.2
- kinetic parameters for redox reactions see § 4.4.2

**Input Waters.** In the experiments, the inflow water was taken from Lake Tegel as discussed in § 2.1. Based on the analyzed water composition (raw data) input waters for the reactive transport model has been generated by PHREEQC. These ‘synthetic’ waters are free of charge-balance errors,  $\Delta IB = 0$ , and stay in equilibrium with mineral phases (see § 3.3).

The so prepared water composition, exemplary for Col 5, is listed in Tab. 2.5. The inflow waters (model input) of the other columns differ only slightly from these data.

**Tab. 2.5** Inflow water of Col 5 (model input generated with PHREEQC).

inflow water Col 5		not ozonated	ozonated
pH	-	8.0	8.0
pe	-	6.6	12.6
T	°C	25	25
Ca	mg/L	104	104
Mg	mg/L	14.3	14.3
Na	mg/L	39.5	39.5
K	mg/L	6.6	6.6
S(6)	mg/L	168	168
C(4)	mg/L	36.4	36.4
Cl	mg/L	54.9	54.9
Fe	mg/L	$2 \cdot 10^{-9}$	$2 \cdot 10^{-9}$
Al	mg/L	0.11	0.11
N(-3)	mg/L	0	0
N(3)	mg/L	0.88	0
N(5)	mg/L	6.7	7.9
P	mg/L	0.006	0.006
Si	mg/L	0.11	0.11
F	mg/L	0.4	0.4

**Inflow Regime.** There are three types of inflow waters:

- **LT**                   unprepared Lake Tegel water
- **LT\_O3**             ozonated Lake Tegel water
- **LT\_tracer**       ozonated Lake Tegel water with 10 mg/L LiBr (see below)

During the experiments the *inflow* water changes according to a predefined time regime:

**LT** ⇒ **LT\_O3** ⇒ **LT\_tracer** ⇒ **LT\_O3** ⇒ **LT**

The start and end times of each interval vary slightly from column to column. The specific time regime of each column test (as defined in [TUB11]) was considered in TRN explicitly.

Tab. 2.5 shows the composition of the non-ozonated and the ozonated water, **LT** and **LT\_O3**. Both waters differ by the pe value (redox potential) and the N speciation (i.e. how N disproportionates into nitrate, nitrite, and ammonium). The relation between pe value and redox potential  $E_h$  is defined in Eq. (4.6) and Eq. (4.7), respectively.

*Remark.* Ozonated water is not stable. The ozone (self-)decay was simulated by a modification of the inflow waters.

**Tracer.** In all column tests LiBr was used as tracer. It has been injected with a uniform concentration of

$$\text{LiBr} = 10 \text{ mg/L}$$

The start time  $t_1$  and injection interval,  $t_2 - t_1$ , was different in each column test:

Col 2:	$t_1 = 164 \text{ h}$	⇒	$t_2 = 235 \text{ h}$	(3 days)
Col 3:	$t_1 = 99 \text{ h}$	⇒	$t_2 = 124 \text{ h}$	(1 day)
Col 4:	$t_1 = 309 \text{ h}$	⇒	$t_2 = 341 \text{ h}$	(1½ day)
Col 5:	$t_1 = 98 \text{ h}$	⇒	$t_2 = 125 \text{ h}$	(1 day)

**Initial Water.** The *initial* water which enters each column cell at  $t = 0$  was chosen as the unprepared Lake Tegel water, **LT**.

## 2.2.4 Thermodynamic Database

PHREEQC, which is embedded in the reactive transport model, uses the standard database *wateq4f*. For transparency reasons, this database is applied in its original form. Additional species that are not contained in *wateq4f* are added to the PHREEQC input files as header (the same header for all PHREEQC calculations during running TRN). Thus, we never change or disturb the original database file ‘wateq4f.dat’.



### 3 HYDRAULICS AND HYDROCHEMISTRY

#### 3.1 Advection and Dispersion

The breakthrough of the tracer ‘LiBr’ was used to check and adjust the hydraulic parameters. More precisely, only the anion Br<sup>-</sup> is the tracer *per se* whereas the cation Li<sup>+</sup> undergoes ion exchange (see Fig. 3.1 and § 3.2).

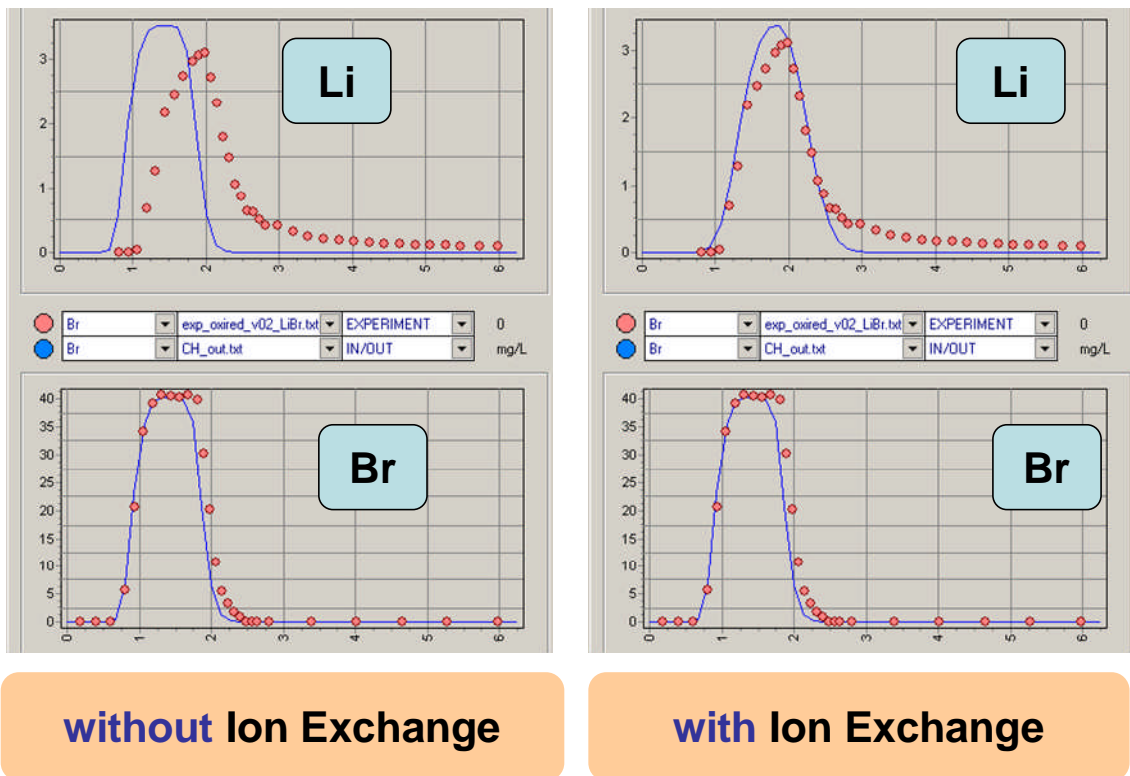


**Fig. 3.1** Calculated and measured breakthrough of Li<sup>+</sup> and Br<sup>-</sup> in Col 2; model without and with ion exchange – blue curves, experiment – red dots (screenshots of TRN).

An optimal description of bromide Br<sup>-</sup> was achieved (in all column tests) by the following parameter set:

volumetric flow	Q = 1.0 to 1.3 mL/min (depends on column test)
pore volume	ε = 0.35
longitudinal dispersivity	α <sub>L</sub> = 0.3 cm

These parameters are used in all calculations of the present study. The dispersivity α<sub>L</sub> enters the Advection-Dispersion equation via the longitudinal dispersion coefficient:

$$(3.1) \quad D_L = \alpha_L v$$

Fig. 3.2 shows how an increase of the longitudinal dispersion  $\alpha_L$  smoothes the bromide breakthrough curves in Col 3. The simulation starts with pure advection, i.e.  $\alpha_L = 0$ , where there is no smoothing at all (due to the fact that the model is free of numerical dispersion).

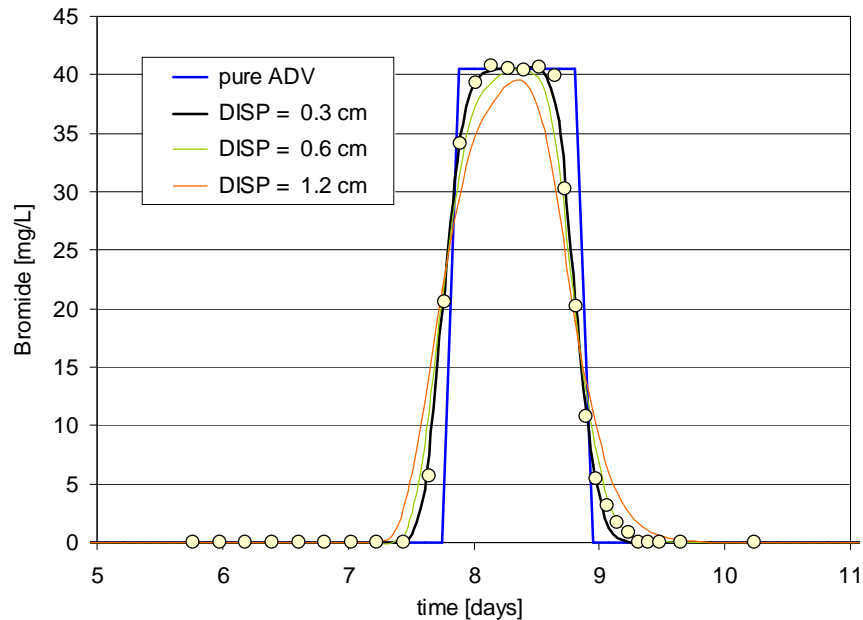
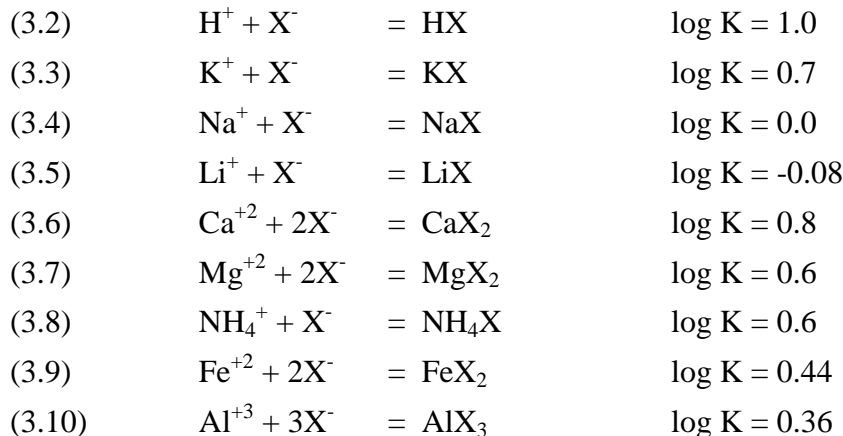


**Fig. 3.2** Tracer 'Bromide' in Col 3 simulated with different longitudinal dispersions  $\alpha_L$  ( $\alpha_L = 0$  is pure advection).

### 3.2 Cation Exchange

Any natural sediment contains at least small amounts of clay or other minerals (rather than pure quartz  $\text{SiO}_2$ ). Clays give reason for ion exchange. Therefore, in all calculations ion exchange of the cations  $\text{H}^+$ ,  $\text{K}^+$ ,  $\text{Na}^+$ ,  $\text{Ca}^{2+}$ ,  $\text{Mg}^{2+}$ ,  $\text{Li}^+$ , and  $\text{NH}_4^+$  is taken into account. They are defined by the following reactions (with log K values from *wateq4f*):



Since the Fe and Al concentrations in the inflow solution are below the detection limit ion exchange of  $\text{Fe}^{+2}$  and  $\text{Al}^{+3}$  plays a minor role only. Nonetheless, these processes are not excluded from calculations. Instead, it was assumed that the (very small) Fe and Al concentrations are in equilibrium with  $\text{FeOOH}$  (goethite) and  $\text{Al}_2\text{Si}_2\text{O}_5(\text{OH})_4$  (kaolinite).

**CEC.** Besides the thermodynamic data (log *k* values from wateq4f) the reactive transport model requires the input parameter ‘total cation capacity per pore volume’:

$$(3.11) \quad C_{\text{TOT}}^{(\text{pore})} = \frac{n_{\text{sites}}}{V_{\text{p}}} = \frac{\text{CEC} \cdot m_{\text{clay}}}{V_{\text{p}}} = \frac{C_{\text{TOT}}}{\varepsilon}$$

where  $n_{\text{sites}}$  is the number of exchanger sites in meq and  $V_{\text{p}}$  is the pore volume. The cation exchange capacity, CEC, of a typical (dry) clay mineral, such like Montmorillonite, is

$$(3.12) \quad \text{CEC} = \frac{n_{\text{sites}}}{m_{\text{clay}}} \approx 90 \frac{\text{meq}}{100 \text{ g}}$$

Assuming a low clay content of 1 wt%, that is,  $f = m_{\text{clay}}/m_{\text{sed}} = 0.01$  where  $m_{\text{sed}}$  is the dry sediment mass with density  $\rho_{\text{B}} \approx 1.7 \text{ g/cm}^3$ , we obtain as a first approximation

$$(3.13) \quad C_{\text{TOT}} = f \cdot \rho_{\text{B}} \cdot \text{CEC} \approx 15 \frac{\text{meq}}{\text{L}} \quad \text{‘theoretical value’}$$

In the model calculations we used  $C_{\text{TOT}} = 15 \text{ meq/L}$  as the start value (prior to the comparison with the experiment). The comparison of the calculated and measured breakthrough of  $\text{Li}^+$  was then used to adjust  $C_{\text{TOT}}$  properly. In general, the higher  $C_{\text{TOT}}$  the higher is the retardation.

**Results.** The adjusted values of  $C_{\text{TOT}}$  are the following (see Fig. 3.3):

- Col 2:  $C_{\text{TOT}} = 20 \text{ meq/L}$
- Col 3:  $C_{\text{TOT}} = 20 \text{ meq/L}$
- Col 4: experimental data for  $\text{Li}^+$  violate mass balance
- Col 5:  $C_{\text{TOT}} = 5 \text{ meq/L}$  (CEC shrinks due to 550°C treatment)

There is a good agreement between the rough ‘theoretical’ prediction in Eq. (3.13) and the extracted  $C_{\text{TOT}}$  values. Also,  $C_{\text{TOT}}$  becomes smaller in the sediment pretreated with 550 °C due to the temperature-driven artificial weathering. Col 5 shows a smaller retardation.

The experimental data of Col 4 (shown in the middle-left diagram of Fig. 3.3) are too small in comparison to the prediction (independent of any particular choice for  $C_{\text{TOT}}$ ). Here, the mass balance deficiency of approximately 50 %, calculated from the area beneath the measured data points, remains an open question. The argument that  $\text{Li}^+$  is fixed by HFO complexes of the iron-coated sand is not supportable since such an HFO-effect is not seen in Col 5 that contains iron coated sand as well.

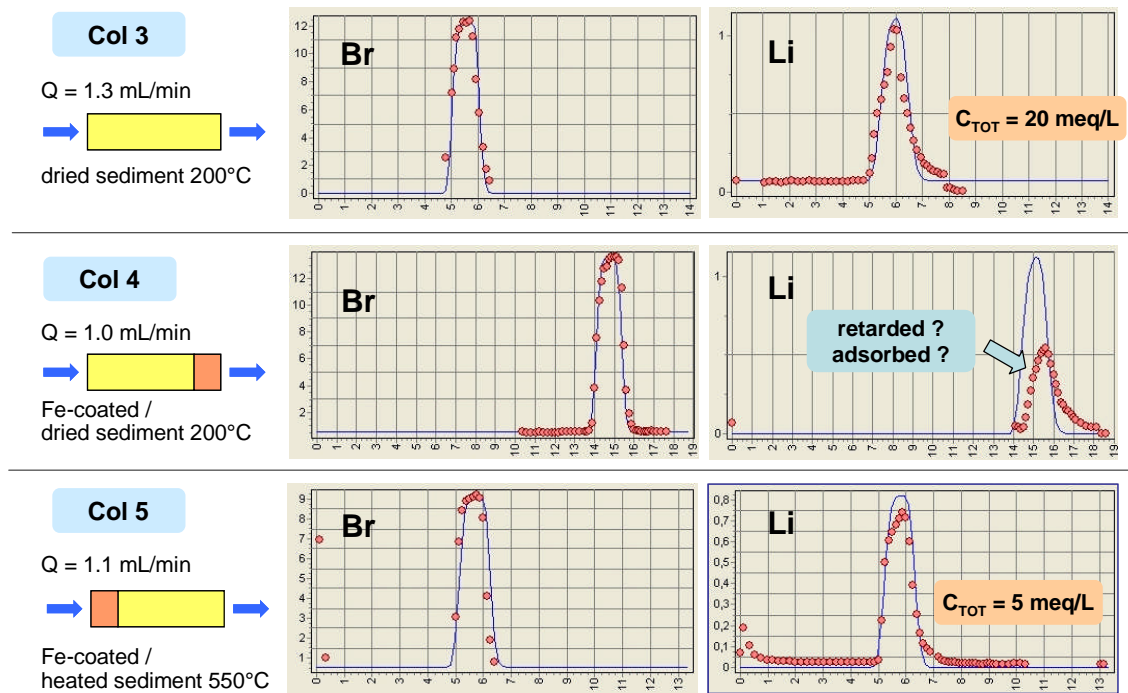


Fig. 3.3 Calculated and measured breakthrough of  $\text{Li}^+$  in Col 3, Col 4, and Col 5; model with ion exchange – blue curves, experiment – red dots (screenshots of TRN).

Tab. 3.1 Sorbed cations on ion exchanger (Col 4)

IX species	concentration [meq/L]
HX	$9 \cdot 10^{-5}$
KX	0.173
NaX	0.326
$\text{CaX}_2$	17.18
$\text{MgX}_2$	2.319
$\text{FeX}_2$	~ 0
$\text{AlX}_3$	~ 0
$\text{NH}_4\text{X}$	~ 0
$\text{LiX}$	~ 0
$\text{C}_{\text{TOT}}$	20.0

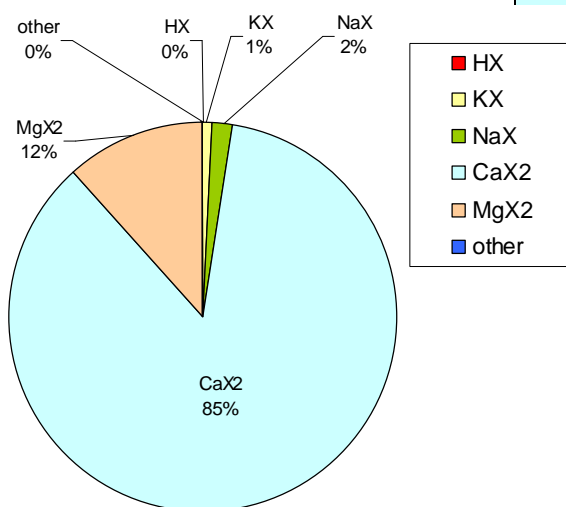


Fig. 3.4 Pie chart of sorbed cations on ion exchanger in Col 4 (data from Tab. 3.1).

Tab. 3.1 shows the distribution of cations on the ion exchanger that is in equilibrium with Lake Tegel water (without LiBr tracer). The partial concentrations sum up to the total exchange capacity  $C_{TOT} = 20$  meq/L. Please note that up to 85 % of the ion exchanger is occupied by Ca.

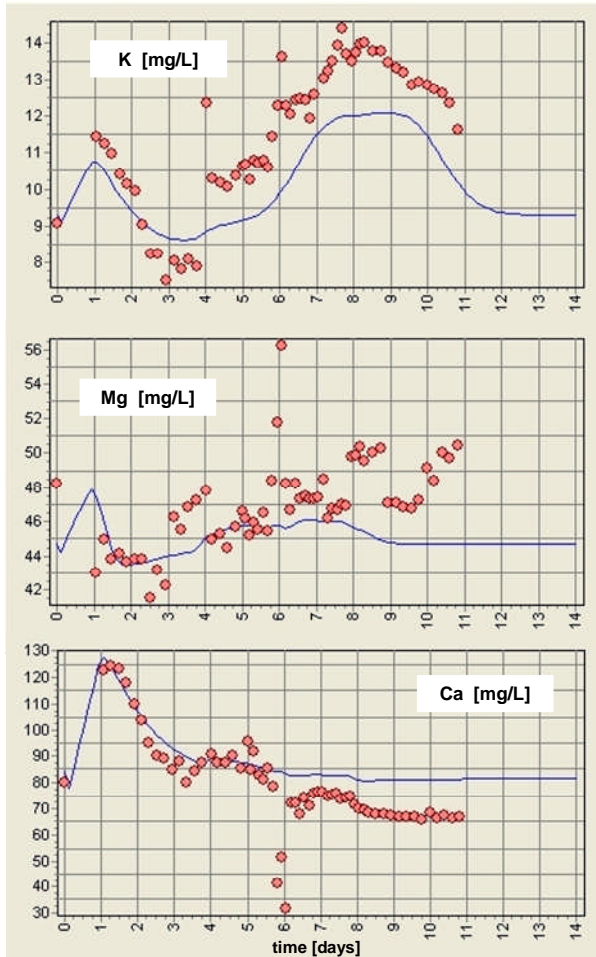


Fig. 3.5 displays the outflow concentrations of K, Mg, and Ca in Col 3. K as a non-reactive element can only be influenced by ion exchange (like Li). Thus, the interesting behavior of K in the upper diagram is caused by loading and deloading of the other major ions like Ca and Mg (Note: the Ca concentration is one order of magnitude higher than the K concentration). The behavior of Ca is affected by pH and the mineral phase calcite as it will be discussed in § 3.3.2.

**Fig. 3.5** Outflow concentrations of K, Mg, and Ca in Col 3 (model calculations and experiments).

### 3.3 Mineral Phases

#### 3.3.1 Theoretical Background

In principle, there are two possibilities to simulate the dissolution and precipitation of minerals:

- by kinetics (based on a kinetic approach and additional parameters)
- by thermodynamics (based on log  $k$  values contained in the PHREEQC database)

The advantage of the equilibrium approach is that it relies on fundamental thermodynamic data rather than on empirical kinetic data (which are less known and in most cases not available).

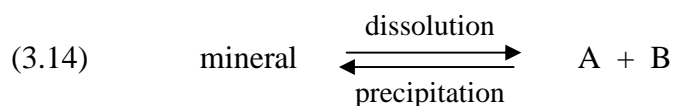
Accordingly, it is quite useful to separate between *reactive* (or primary) and *secondary* minerals:

- reactive minerals (dissolution only)
- secondary minerals (precipitation and dissolution)

Reactive minerals act as a source; secondary minerals act mainly as a sink for elements. Therefore, reactive minerals require an initial mass  $m_0$  (more precisely: the initial amount  $n_0$  of moles per liter solution). Whereas reactive minerals are predestinated for a kinetic approach secondary minerals are described as reversible processes controlled by equilibrium thermodynamics.

Though the separation between reactive and secondary minerals is very convenient for conceptual models, in natural systems there is no such sharp borderline. Typical reactive minerals are pyrite, clay minerals and carbonates (calcite, dolomite); typical secondary minerals are gypsum, amorphous hydroxides like  $\text{Fe}(\text{OH})_3$  and  $\text{Al}(\text{OH})_3$ , and calcite. Thus, calcite can be assigned as a reactive or a secondary mineral. In the present study we use a kinetic approach for calcite – see Eqs. (3.18) and (3.19).

**IAP and SI.** The dissolution and precipitation of a mineral phase, AB, is given by the reaction formula



For example, in case of calcite,  $\text{CaCO}_3$ , A and B symbolize  $\text{Ca}^{+2}$  and  $\text{CO}_3^{-2}$ . The activities of reactants A and B *at equilibrium* defines the equilibrium constant

$$(3.15) \quad K = [\text{A}]_{\text{eq}} [\text{B}]_{\text{eq}} \quad (\text{equilibrium constant})$$

On the other hand, the *measured* activities define the ion activity product

$$(3.16) \quad \text{IAP} = [\text{A}]_{\text{actual}} [\text{B}]_{\text{actual}} \quad (\text{ion activity product})$$

The saturation index is then defined by

$$(3.17) \quad SI = \log\left(\frac{IAP}{K}\right) \quad (\text{saturation index})$$

According to the SI value we distinguish between three cases:

- |        |                                    |                  |
|--------|------------------------------------|------------------|
| SI = 0 | solution is <i>saturated</i>       | with the mineral |
| SI < 0 | solution is <i>under-saturated</i> | with the mineral |
| SI > 0 | solution is <i>supersaturated</i>  | with the mineral |

If SI < 0 we have IAP < K and the reaction in Eq. (3.14) will proceed to the right (dissolution). Vice versa, if SI > 0 we have IAP > K and the reaction will proceed to the left (precipitation).

### 3.3.2 Model Calculations

With regard to ‘reactive minerals’ the columns represent a simple system. The sediment used in the experiments is in equilibrium with the solution (lake water) and long-term weathering processes do not need to be considered in these short-term tests. Therefore no ‘*primary* minerals’ are considered in the model. However, ‘*secondary* minerals’ that could precipitate from the solution have been included in all calculations:

- |                              |                        |   |                       |
|------------------------------|------------------------|---|-----------------------|
| • gypsum                     | <chem>CaSO4.H2O</chem> | } | as equilibrium phases |
| • ferrihydrite               | <chem>Fe(OH)3</chem>   |   |                       |
| • aluminum hydroxide         | <chem>Al(OH)3</chem>   |   |                       |
| • amorphous SiO <sub>2</sub> | <chem>SiO2(am)</chem>  |   |                       |
| • calcite                    | <chem>CaCO3</chem>     |   | as kinetic reaction   |

From these minerals only *calcite* affects the water composition significantly (see Fig. 3.6); calcite is treated as a kinetic reaction. The other minerals enter the model as ‘equilibrium phases’ based on log k values (taken from the PHREEQC’s standard database *wateq4f*). However, the influence of these equilibrium phases is negligible in the column tests; only small amounts (if any) precipitate.

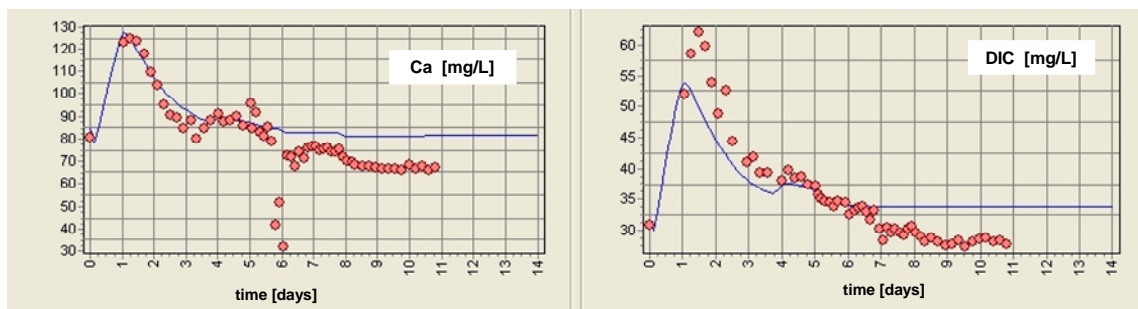


**Fig. 3.6** Ca and DIC in the outflow solution in Col 3 (model calculations and experiments).

The extraordinary role of calcite already becomes clear from the hydrochemistry of the inflow water from Lake Tegel: This water is supersaturated with calcite, what calls for a kinetic description.

**Calcite Kinetics.** The dissolution and precipitation of calcite is treated as ‘higher-order kinetics’ depending on the saturation index, SI (see also Eq. (A.12), [PA99]):

$$(3.18) \quad \left. \frac{1}{V} \frac{dm}{dt} \right|_{\text{diss}} = -r_{\text{diss}} \cdot (1 - 10^{\text{SI}}) \cdot \left( \frac{m}{m_0} \right) \quad \text{for } \text{SI} < 0$$

$$(3.19) \quad \left. \frac{1}{V} \frac{dm}{dt} \right|_{\text{prec}} = r_{\text{prec}} \cdot (1 - 10^{\text{SI}}) \quad \text{for } \text{SI} > 0$$

Here,  $m(t)$  and  $m_0$  denote the actual and initial amount of calcite in mol;  $V$  is the solution volume, and  $r_{\text{diss}}$  and  $r_{\text{prec}}$  are the specific dissolution and precipitation rates:

$$r_{\text{diss}} = 3 \cdot 10^{-8} \text{ mol/L/s}$$

$$r_{\text{prec}} = 1 \cdot 10^{-8} \text{ mol/L/s}$$

The initial amount of calcite,  $m_0$ , was fitted to the data (see Tab. 3.2). It represents the *reactive* fraction of the total  $\text{CaCO}_3$  in the sediment, i.e. that part that is in direct contact to the solution. Please note that the precipitation does not depend on the calcite amount  $m$  or  $m_0$ .

**Initial Acidity.** In all column tests a wash-out of ‘weathering products’ was observed just after start. This effect is accompanied (except Col 5) with a steep decrease of pH from about 8.5 to 6 (see red dots in Fig. 3.7). This relatively fast ‘acidification’ cannot be explained neither by mineral dissolution nor by biodegradation alone. It seems to be an artificial effect caused by the pre-treatment/heating of the sediment (weathering of the material due to air contact). In order to simulate this effect we assume a short-term acidification by acids, abbreviated by ‘HA’, that generate  $\text{H}^+$  ions with decreasing rate from  $10^{-7}$  mol/L/s to zero in the first 20 hours (first-order kinetics with an initial amount given in Tab. 3.2).

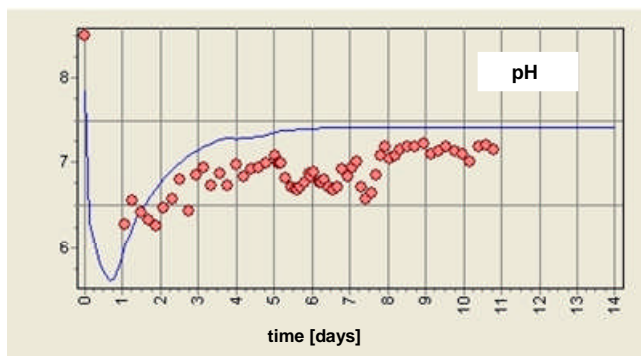


**Fig. 3.7** pH value in the outflow solution in Col 3 (model calculations and experiments).

**Results.** Comparison of model calculations with measured data in Fig. 3.6 and Fig. 3.7 shows the sensitive interrelation between pH, Ca, and DIC (dissolved inorganic carbon) in the outflow solution of Col 3. In particular, small changes of pH strongly affect both Ca and DIC concentrations, and vice versa.

This behavior is typical for all columns but it is best evidenced in Col 3. In Col 2 the Ca values and in Col 4 the DIC values are missing in the time interval just after start. Only Col 5 behaves completely different due to the severe pre-treatment at 550 °C.

**Initial Conditions.** The pre-treatment of the sediment differs from column to column (as indicated in Tab. 2.1). Particularly this variation reflects in the initial amounts of calcite and HA as shown in Tab. 3.2. These parameters are not known beforehand; they were adjusted in model calculations.

initial amount	Calcite [mM]	HA [mM]
Col 2	1	4
Col 3	5	8
Col 4	5	8
Col 5	0	0

**Tab. 3.2** Initial amount of calcite and acidity (HA) in mmol per liter pore solution.

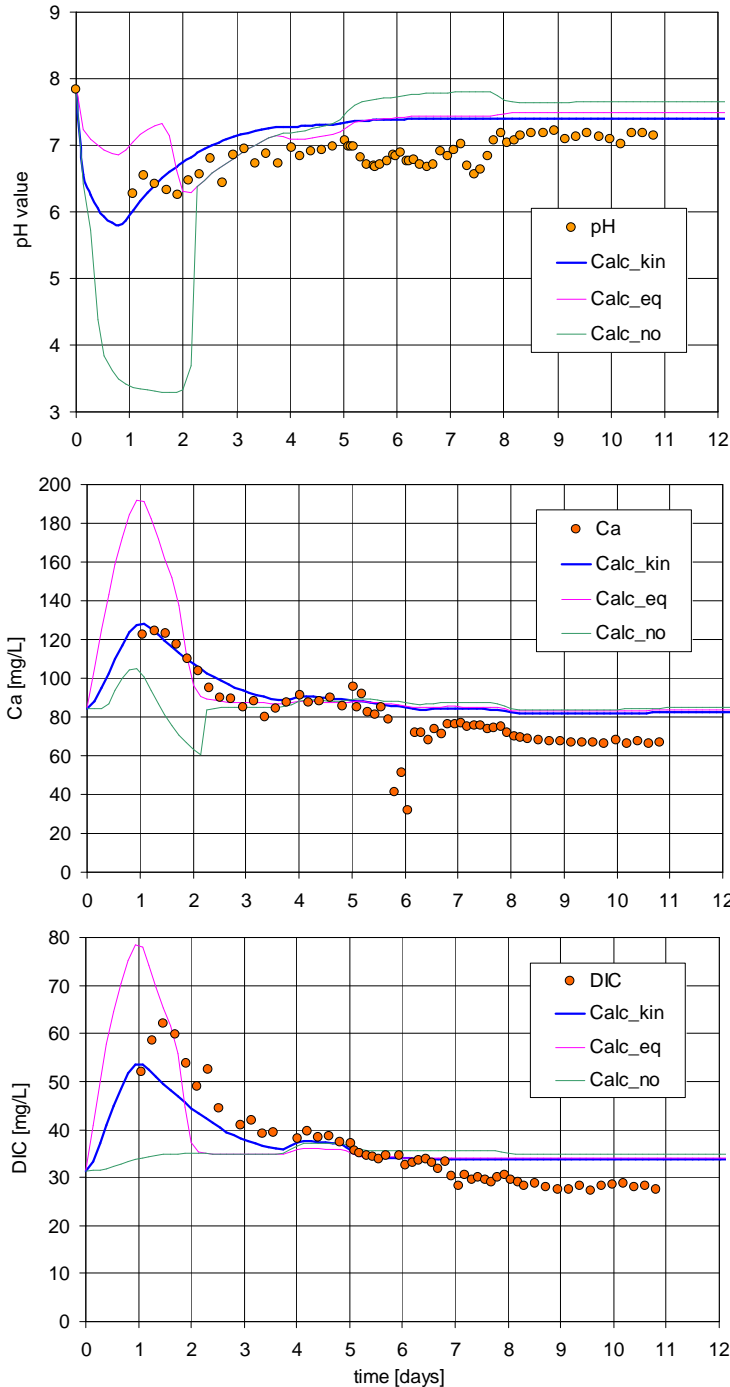
The data in Tab. 3.2 indicate that the amount of calcite in Col 2 (untreated sediment) is smaller than in Col 3 and Col 4. On the other hand, in Col 5 calcite seems to be destroyed by the pre-treatment at 550 °C. The same considerations are valid for the initial acidity potential (HA).

Final Note: Hydrochemical modeling does not allow *separate* adjustment of *one* parameter (i.e. element) without influencing all other parameters. All quantities are tightly connected with each other by *mass* balance and by *charge* balance.

### 3.3.3 Comparison of three Calcite-Precipitation Models

Three precipitation models for calcite are compared:

- kinetic approach (applied and described in § 3.3.2)
- equilibrium approach (based on thermodynamic log K values)
- no calcite / no precipitation



In the equilibrium approach super-saturation of  $SI = 0.5$  is assumed.

The results are shown in Fig. 3.8. The diagrams display pH, Ca, and DIC in the outflow solution of Col 3 (experimental data are marked by red dots). Evidently, the best description is obtained by the kinetic approach (blue curve).

**Fig. 3.8** Comparison of three “calcite precipitation models”: (i) kinetic approach, (ii) equilibrium thermodynamics, (iii) no calcite / no precipitation. The diagrams show are pH, Ca, and DIC in the outflow solution of Col 3 (dots – experimental data).

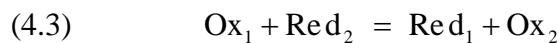
## 4 REDOX REACTIONS

### 4.1 Theoretical Background

Redox reactions are oxidation-reduction reactions. The term *oxidation* refers to the removal of electrons from an atom, forcing an increase in the oxidation number; *reduction* refers to the addition of electrons to lower the oxidation number. Thus, in redox reactions there is always a transfer of electrons from a reducing agent 'Red' (electron donor) to an oxidizing agent 'Ox' (electron acceptor):



which add up to the total reaction equation



Here  $n$  denotes the number of electrons. The electron exchange occurs between so-called redox-sensitive elements, i.e. elements with more than one valence state (oxidation number): C, O, N, S, Fe, Mn, and other trace metals like Mo, Cr, As, Co, Ni, Sb, Th and U. Free electrons do not exist in natural systems, hence, any group of half reactions which add up to the total reaction equation should obey the 'electron balance'.

Redox reactions are mediated by microorganisms. The microorganisms act as catalysts speeding up the reactions that otherwise would be extremely slow. The electron transfer mediated by microbes is sketched in Fig. 4.1.

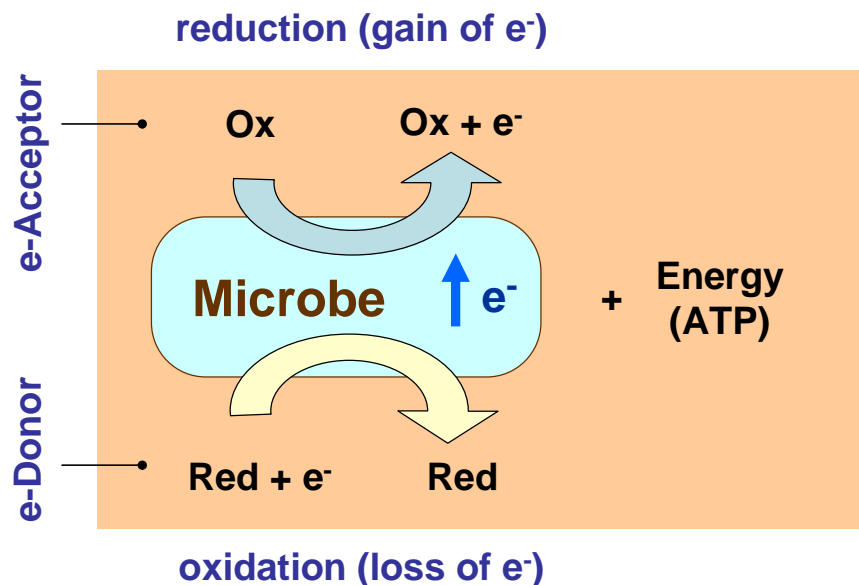


Fig. 4.1 Electron transfer in redox reactions mediated by microorganisms.

Half-redox reactions are similar to other equilibrium reactions. (Please note that the above equations are analogous to acid-base reactions where instead of an *electron* transfer there is a transfer of *protons*,  $H^+$ .) Thus, in parallel to the definition of pH there is a similar definition of pe based on the ‘electron concentration’ or ‘electron activity’  $[e^-]$ :

$$(4.4) \quad \text{pH} = -\log [H^+]$$

$$(4.5) \quad \text{pe} = -\log [e^-]$$

High proton concentration means low pH-values; high ‘electron concentration’ means low pe-values. The relation between the measured redox potential or ORP in V relative to SHE (standard hydrogen electrode), and the pe-value is

$$(4.6) \quad \text{pe} = \frac{F}{\ln 10 \cdot RT} E_h$$

where the FARADAY constant is  $F = 96\,490 \text{ J}\cdot\text{V}^{-1}$  and  $R = 8.314 \text{ J}\cdot\text{mol}^{-1}\cdot\text{K}^{-1}$ . For  $25 \text{ }^\circ\text{C}$  ( $T = 298.15 \text{ K}$ ) the equation simplifies to

$$(4.7) \quad \text{pe} = E_h [\text{V}] / 0.059$$

If some of the half-redox reactions are in equilibrium, redox phenomena can be modeled as equilibrium processes (using PHREEQC-code, for example). However, redox reactions often are slow relative to physical processes (transport, mixing etc.) which call for a kinetic description.

Fig. 4.2 compares schematically redox reactions with acid-base reactions.

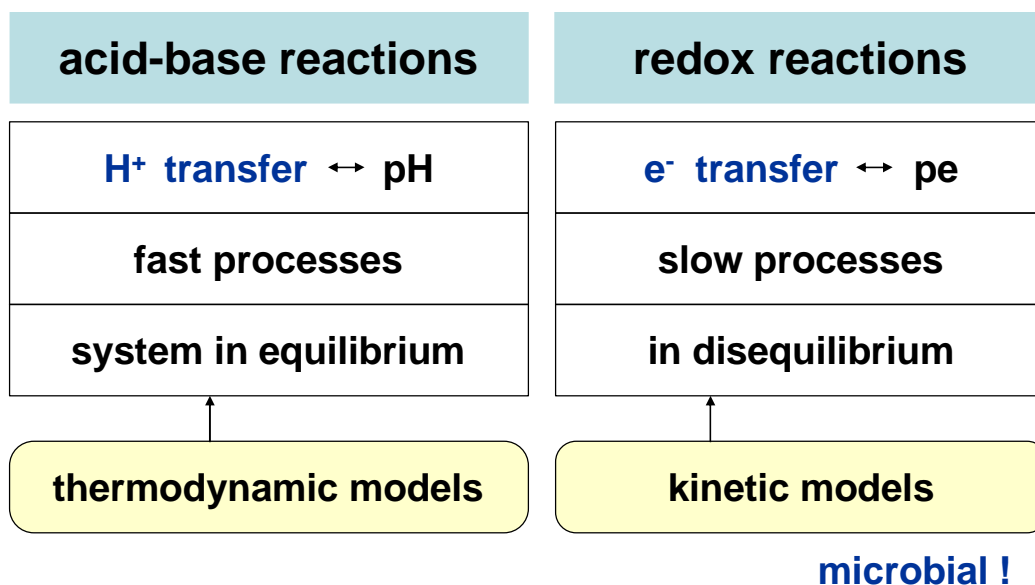
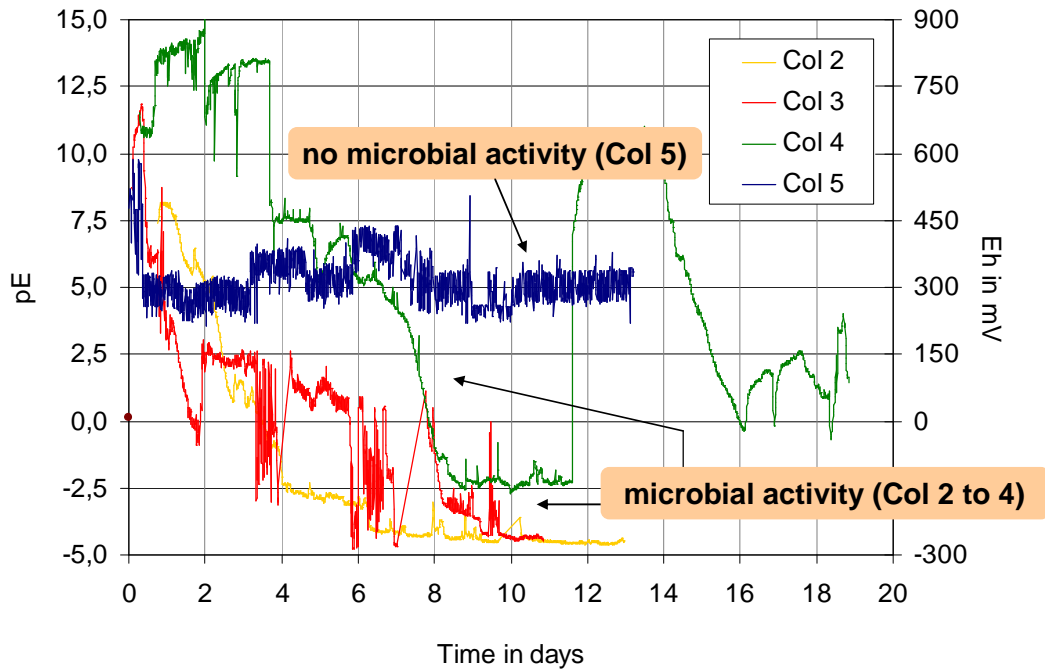


Fig. 4.2 Acid-base reactions versus redox reactions.

## 4.2 Experimental Evidence for Redox Reactions

Redox reactions are, in fact, the central topic of the present OXIRE2 project. In natural systems redox reactions are mediated by microbial activity [KWB10]. In particular, aerobic biodegradation of organic material results in a decrease of the redox potential (Eh or pe value) and pH value. These effects are seen in the column experiments.



**Fig. 4.3** Measured redox potential, Eh or pe, in Col 2 to Col 5.

Fig. 4.3 displays the measured redox potential in the outflow solution of Col 2 to Col 5. After starting the column tests the redox potential drops down from  $pe \approx 10$  to  $-4$  in Col 2 and Col 3, and from  $pe \approx 13$  to  $-2.5$  in Col 4 which is an indicator for microbial activity.

Conversely, there is no evidence for microbial activity in Col 5 (the redox potential remains at ambient oxic conditions at  $pe \approx 5$ ). It seems quite reasonable that the microbial population was damaged during the pre-treating of the sediment at  $550\text{ }^\circ\text{C}$ . Only Col 5 was pretreated at such high temperatures (see Tab. 4.1).

**Tab. 4.1** Column setup used in the experiments.

		Col 1	Col 2	Col 3	Col 4	Col 5
flow Q	mL/min		1.3	1.3	1.0	1.1
sediment		natural	natural	200 °C	200 °C	550 °C
CEC	meq/L	20	20	20	20	5
$\mu$ biology		yes	yes	yes	yes	no
Fe-coated sand		no	no	no	yes	yes

### 4.3 Redox Sequences in the Column Tests

Sequences of redox reactions and redox zoning play a key role in environmental geochemistry [AP05] and, especially, in bank filtration and artificial recharge [KWB10]. Fig. 4.4 displays typical redox sequences at neutral pH. The diagram highlights the half reactions (in orange color) which are relevant for biodegradation in the present column tests. In particular, the system does not contain sufficient manganese and dissolved iron to be relevant.

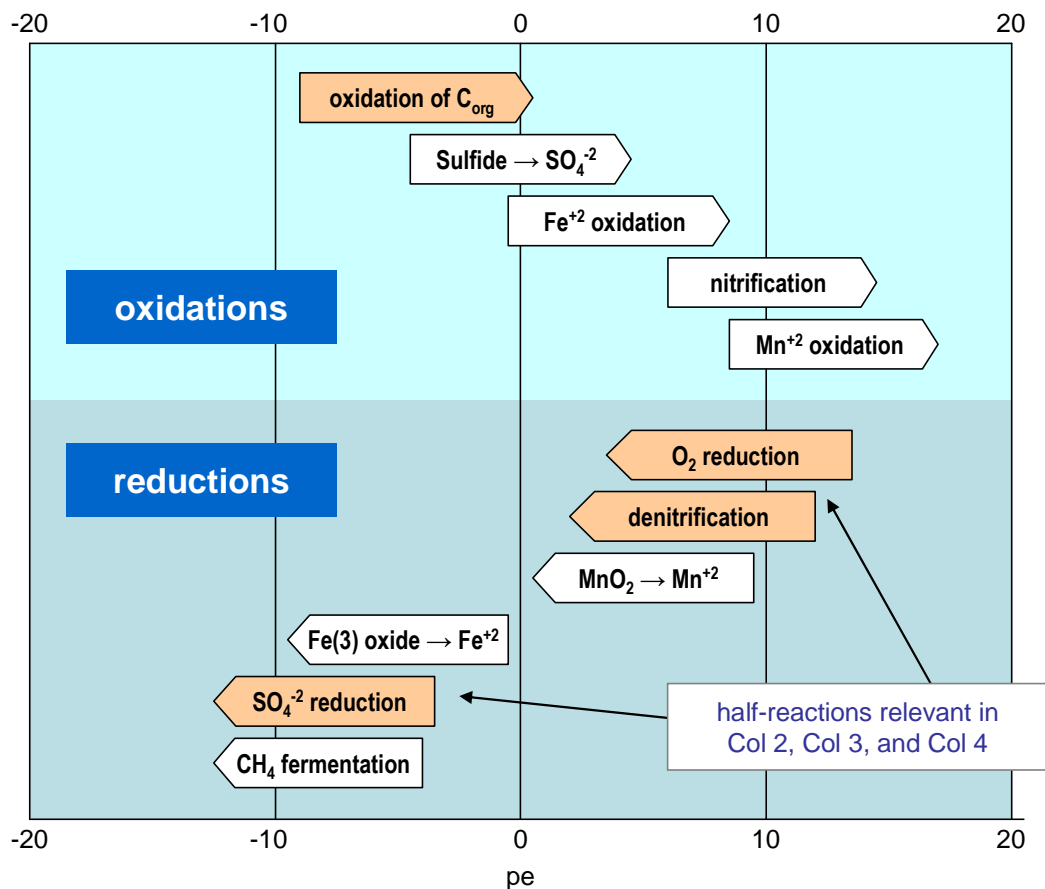
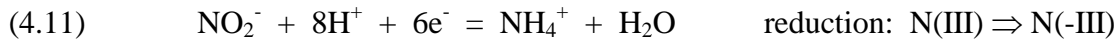
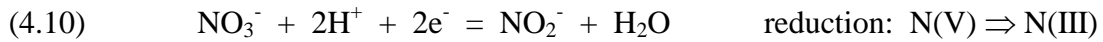


Fig. 4.4 Redox sequences at pH = 7 in natural systems. Half-reactions which are relevant for the biodegradation in the present column tests are marked in orange color.

**e<sup>-</sup> Donor.** All columns contain organic matter (as it is evident from the measured f<sub>OC</sub> values in Tab. 2.3). Thus, the starting point for all further consideration is the biodegradation of organic matter. It is a good approximation to use CH<sub>2</sub>O (i.e. 1/6 glucose) as a common representative for organic matter. In this way, CH<sub>2</sub>O acts as electron donor in the oxidation half-reaction:



**e<sup>-</sup> Acceptors.** There are four potential e<sup>-</sup> acceptors in the column system: oxygen, nitrate, nitrite, and sulfate. The corresponding reduction half-reactions are:



In reality, the reaction pathways are not nearly as simple as considered. For example, the reduction of nitrate to ammonium proceeds via several nitrogen compounds:

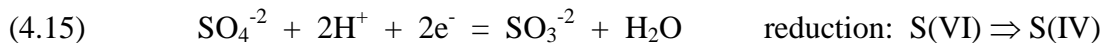


Here, NO<sub>x</sub> abbreviates the gases NO, NO<sub>2</sub>, N<sub>2</sub>O; PON and DON are particular organic nitrogen and dissolved organic nitrogen.

The same holds true for *sulfate* which is reduced in long chain of steps down to sulfide, S(-II), where in total eight electrons are transferred:



For example, the reduction to sulfite is given by



Note: The ‘sulfite chemistry’ defined in Eq. (4.15) is not contained in wateq4f. Thus, we explicitly implemented the ‘sulfite chemistry’ into the model to study this effect.

As it will be shown in the model calculations in § 4.5 the redox processes in the columns are dominated by the major electron acceptors O<sub>2</sub>, nitrate and nitrite alone. The sulfate reduction is too small to be reliably identified by the experimental data (even if the ‘sulfite chemistry’ defined in Eq. (4.15) is considered). Images of redox zonation inside the column are given in Fig. 4.13.

## 4.4 Biodegradation and Enzyme Kinetics

### 4.4.1 Conceptual Model

The biodegradation model bases on a combined approach of enzyme kinetics and thermodynamics. Whereas the degradation of organic matter in Eq. (4.8) is treated by enzyme kinetics the accompanied electron transfer and electron balance is controlled by thermodynamics (using PHREEQC). In PHREEQC all relevant redox reactions are considered *per se*; they are defined in the thermodynamic database (wateq4f) which contains a long list of reaction equations and log K values (equilibrium constants).

**Enzyme Kinetics.** A brief introduction to enzyme kinetics is presented in Appendix B. The set of differential equations that considers both enzyme kinetics and population dynamics is given in Eqs. (B.20) to (B.22):

$$(4.16) \quad \frac{d[S]}{dt} = -\frac{\mu(t)}{Y} \cdot B(t)$$

$$(4.17) \quad \frac{dB}{dt} = \{ \mu(t) - \Gamma \} \cdot B(t)$$

$$(4.18) \quad \mu(t) = \mu_{\max} \frac{[S]}{K_S + [S]}$$

Here, the symbols are:

[S(t)]	substrate concentration	in mol/L
B(t)	biomass concentration	in cells/L
$K_S$	half-saturation constant	in mol/L
$\mu_{\max}$	maximum rate	in 1/s
$\Gamma$	cell death rate	in 1/s
Y	yield coefficient	in cells/mol

This submodel contains at least four parameters which are not known beforehand:  $\mu_{\max}$ ,  $K_S$ ,  $\Gamma$  and Y (as well as the initial biomass concentration  $B_0$ ). The number of experiments, however, is too small in order to fit all these parameters reliably. Hence, some simplifications will be done below.

The enzyme kinetics is applied for the oxidation of organic matter defined in Eq. (4.8), i.e. the substrate is  $\text{CH}_2\text{O}$ . Inserting Eq. (4.18) into Eq. (4.16) we get

$$(4.19) \quad \frac{d[\text{CH}_2\text{O}]}{dt} = -\mu_0 \frac{[\text{CH}_2\text{O}]}{K_S + [\text{CH}_2\text{O}]} \cdot \left( \frac{B(t)}{B_{\max}} \right) \quad \text{with} \quad \mu_0 = \frac{\mu_{\max}}{Y} \cdot B_{\max}$$

**Population Dynamics.** The population dynamics,  $B(t)$ , is used to simulate the lagtime behavior of the microorganisms (at  $t = 0$  it starts with  $B_0 \approx 0$ ). Instead of solving the differential equation (4.17) numerically (whereby  $\Gamma$  is an unknown parameter) we use an analytical closed-form expression. It is assumed that the active biomass grows from zero to a saturation level  $B_{\max}$  according to a smooth step function:

$$(4.20) \quad \frac{B(t)}{B_{\max}} = \left[ 1 + \exp\left( \frac{t_{\text{lag}} - t}{\Delta} \right) \right]^{-1}$$

where  $t_{\text{lag}}$  is the lagtime and  $\Delta$  a smoothing parameter. As shown in Fig. 4.5 this ‘normalized’ function starts at zero and switches to 1 when the time comes near the lag time,  $t \approx t_{\text{lag}}$ . The parameter  $\Delta$  controls how steep or smooth the transition from 0 to 1 is (the larger  $\Delta$  the broader the transition).

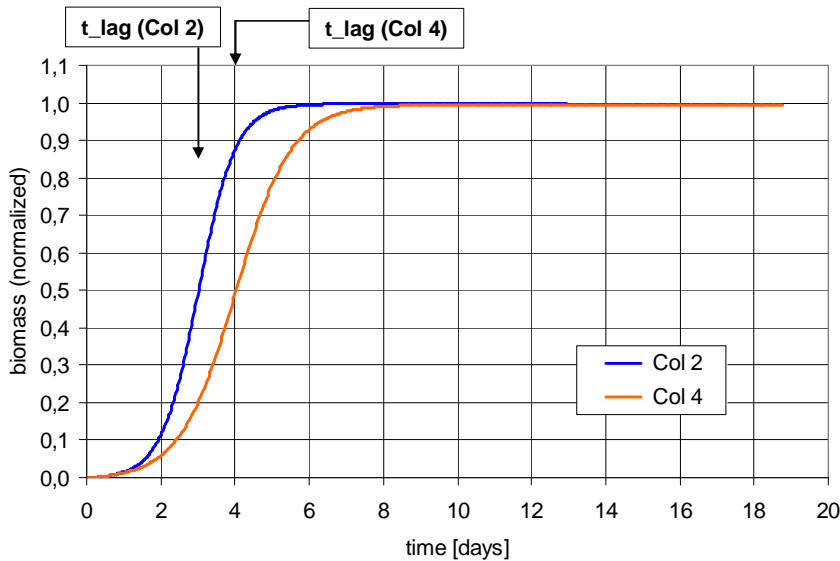


**Fig. 4.5** Population dynamics in Col 2 and Col 4 expressed by the 'normalized' biomass concentration  $B(t)/B_{\max}$  in Eq. (4.20).

**e Acceptors.** So far Eq. (4.19) works for conditions where the supply of electron acceptors in the system is time-independent. In practice, however, the amount of e-acceptors (oxygen, nitrate, and nitrite) varies strongly over time. The higher the amount of e-acceptors the faster the organic material degrades (no e-acceptors – no degradation). Thus, it is assumed that the biodegradation rate is proportional to the amount of all e-acceptors actually present in the system, especially  $O_2(t)$ ,  $NO_3^-(t)$  and  $NO_2^-(t)$ . Mathematically, the *constant* rate parameter  $\mu_0$  in Eq. (4.19) is replaced by a time-dependent one:

$$(4.21) \quad \mu_0 \quad \Rightarrow \quad \mu_0(t) = \mu_{\text{eff}} \cdot f_{\text{accept}}(t)$$

with

$$(4.22) \quad f_{\text{accept}}(t) = f_0 + a_0 [O_2(t)] + a_1 [NO_3^-(t)] + a_2 [NO_2^-(t)]$$

Here, the coefficients are chosen as  $a_0 = a_1 = 1 \text{ mol}^{-1}$  and  $a_2 = \frac{1}{2} a_1$ . In addition, the tiny 'background factor'  $f_0 = 1 \cdot 10^{-5}$  accounts for all other minor e-acceptors in the column system (sulfate, redox specific metal ions, etc.). The  $a_i$  coefficients are chosen as 1.

[Note: In the experiments  $O_2$  is always accompanied with nitrate. Thus, in order to keep the parameter number as small as possible  $O_2$  and  $NO_3^-$  are lumped together into one term of Eq. (4.22).]

Eq. (4.19) with  $\mu_0(t)$  is used to calculate at each time step  $t_i$  and in each column cell  $x_n$  the amount  $\Delta m$  of  $CH_2O$  that is biodegraded. The electrons released in this *oxidation* reaction are captured by electron acceptors like  $O_2$ , nitrate and/or nitrite (which undergo a *reduction* process).

#### 4.4.2 Model Parameters and Initial Conditions

**Parameter Adjustment.** The biodegradation model defined by Eqs. (4.19) to (4.21) contains four main parameters:

$\mu_{\text{eff}}$	effective rate	in mol/L/s
$K_S$	half-saturation constant	in mol/L
$t_{\text{lag}}$	lag time	in h
$\Delta$	time parameter	in h

These four parameters were adjusted to get an optimal description of the time development of 7 *measured* quantities: pe value, dissolved oxygen, nitrate, nitrite, ammonium, as well as pH and DIC. The so obtained ‘best-fit’ parameter set is listed in Tab. 4.2.

**Tab. 4.2** Parameter set for enzyme kinetics (extracted from column tests)

column	sediment (preparation)	$\mu_{\text{eff}}$	$K_S$	$t_{\text{lag}}$	$\Delta$
		mol/L/s	mmol/L	hours	hours
Col 2	natural	$4 \cdot 10^{-7}$	8	72	12
Col 3	200 °C	$4 \cdot 10^{-7}$	8	36	18
Col 4	200 °C	$4 \cdot 10^{-7}$	8	96	18
Col 5	550 °C	$0.4 \cdot 10^{-7}$	0.05	4	3

As discussed in § 4.2, microbial activity is expected in Col 2, Col 3, and Col 4, but it is damaged in Col 5 due to the heating of sediment at 550 °C. Nonetheless, Col 5 was not excluded from the redox calculations; the extracted parameter set for Col 5, however, may be not very meaningful. The major premise in performing the parameter fit was that the two MICHAELIS-MENTEN parameters  $\mu_0$  and  $K_S$  should be equal in all ‘microbial active’ columns, i.e. in Col 2, Col 3, and Col 4. This was, in fact, achieved as shown in Tab. 4.2.

**Initial Conditions.** In addition to the four model parameter the two differential equations (4.19) and (4.20) require two initial conditions for  $t = 0$ :

$[\text{CH}_2\text{O}]_0$	initial mass of reactive $\text{CH}_2\text{O}$	in mol/L
$B_0 = 0$	initial biomass	in mol/L

An estimation for the initial organic matter which is accessible and degradable by microorganisms  $[\text{CH}_2\text{O}]_0$ , follows from the measured TOC in the sediment (before and after the column test). As shown below, the maximum *degraded* TOC is in the order of 40 mM carbon (result of measurement at the column entrance, but keep in mind the measure accuracy). The *degradable* TOC inside the columns should be larger than this value. In particular, assuming an initial mass  $[\text{CH}_2\text{O}]_0$  of, say, 80 mM we observed in the calculations that only a small amount (of about 5 % as an average over the whole

column) is degraded during the experimental time. At the column entrance, however, the degraded organic matter is higher.

In summary, we used the following initial conditions:

$$(4.23) \quad [\text{CH}_2\text{O}]_0 = 80 \text{ mM} \quad (\text{and } 5 \text{ mM for Col 5})$$

$$(4.24) \quad B_0 = 0$$

**TOC in Sediment.** The sediment is characterized by the following parameters (typical assumptions for sandy sediments because they were not measured):

$$(4.25) \quad \text{porosity} \quad \varepsilon = 0.35 \text{ m}^3/\text{m}^3$$

$$(4.26) \quad \text{grain density} \quad \rho_S = 2.6 \text{ g/cm}^3 \quad (\text{quartz sand})$$

$$(4.27) \quad \text{dry density} \quad \rho_{\text{dry}} = \rho_S (1 - \varepsilon) = 1.7 \text{ g/cm}^3$$

$$(4.28) \quad \text{wet density} \quad \rho_{\text{wet}} = \rho_{\text{dry}} + \varepsilon \rho_W = 2.0 \text{ g/cm}^3$$

Here,  $\rho_W = 1 \text{ g/cm}^3$  is the density of water. The amount of TOC in the sediments is listed in Tab. 2.3. The average value of Col 2, Col 3 and Col 4 is in the order of 0.17 to 0.18 wt%:

$$(4.29) \quad \text{average TOC content} \quad x_{\text{TOC}} \approx 0.18 \text{ wt\%} = 0.0018 \text{ g/g}$$

$$(4.30) \quad \text{degraded TOC} \quad \Delta x_{\text{TOC}} \approx 0.01 \text{ wt\%}$$

The ‘degraded TOC’ is the difference between the measured TOC before and after the column test in Col 3:  $0.17 \text{ wt\%} - 0.16 \text{ wt\%} = 0.01 \text{ wt\%}$ . (For Col 2 and Col 4 the final TOC content was not measured, and therefore  $\Delta x_{\text{TOC}}$  values are not available.)

The aim is now to translate the measured TOC content into concentration (i.e. into moles of carbon per liter pore solution). For this purpose we use the relation:

$$(4.31) \quad [\text{TOC}] = \frac{m_{\text{TOC}}}{V_p} = \frac{x_{\text{TOC}} m_{\text{dry}}}{V_p} = \frac{x_{\text{TOC}} \rho_{\text{dry}} V_{\text{col}}}{\varepsilon V_{\text{col}}} = \frac{x_{\text{TOC}} \rho_{\text{dry}}}{\varepsilon}$$

where  $V_p$  and  $V_{\text{col}}$  are the pore and column volumes. Using the above parameters for the degraded TOC of  $\Delta x_{\text{TOC}} = 0.01 \text{ wt\%}$  and the molar weight of carbon,  $M_r = 12 \text{ g/mol}$ , one gets:

$$(4.32) \quad [\text{TOC}]_{\text{deg}} = \frac{0.0019 \cdot 1.7 \text{ g}}{0.35 \text{ cm}^3} = 0.5 \cdot 10^{-3} \frac{\text{g}}{\text{cm}^3} = 40 \frac{\text{mmol}}{\text{L}}$$

**Thermodynamics & Kinetics.** Fig. 4.6 sketches the idea behind the interplay of thermodynamics and kinetics in the applied model. The biodegradation of  $\text{CH}_2\text{O}$  is simulated by enzyme *kinetics*. Each molecule of  $\text{CH}_2\text{O}$  releases 4 electrons which are immediately captured by  $e^-$  acceptors ( $\text{O}_2$ ,  $\text{NO}_3^-$ ,  $\text{NO}_2^-$ ). The latter process is completely controlled by *thermodynamics* (where the reaction stoichiometry and  $\log K$  values are defined in the PHREEQC database wateq4f). The so modified concentrations of the redox species ( $e^-$  acceptors) influence then, via the rate coefficient  $\mu_0(t)$ , the degradation process. In this way, the system represents a nonlinear feedback loop.

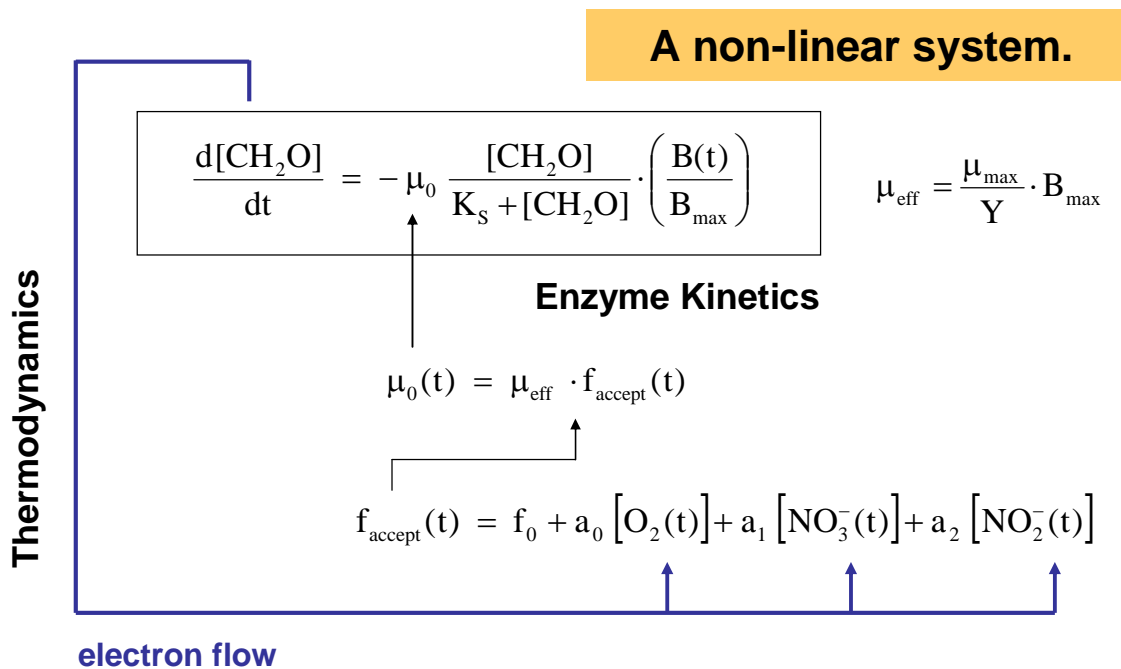


**Fig. 4.6** Interplay of thermodynamics and kinetics in the present model: Nonlinear feedback loop connected by electron balance.

## 4.5 Application and Model Results

### 4.5.1 Model Calculations versus Experiments

The simulation of the redox processes is based on the biodegradation model in Eqs. (4.19) to (4.21) and the parameter set in Tab. 4.2. In the following we focus on the pe value (ORP) and the redox species:

- dissolved oxygen            O(0)
- nitrate                        N(5)
- nitrite                        N(3)
- ammonium                    N(-3)

[All other elements are already discussed in the foregoing Chapters.] The measured and calculated outflow concentrations of these four redox species are shown in the diagrams of Fig. 4.7 (for Col 2), in Fig. 4.8 (for Col 3), in Fig. 4.9 (for Col 4), and in Fig. 4.10 (for Col 5). In addition, pH and the pe values for all columns are displayed in Fig. 4.11. In all cases the model fits the general trend of the experimental data.

From the mathematical point of view, the underlying system is highly *non-linear*. Just small changes of one single element concentration cause huge changes of the pe value. This effect is observable, for example, in the pe diagrams of Fig. 4.11. In this way, the numerical simulation of redox reactions belongs to the most complicated tasks in hydro-chemistry. In order to understand the ongoing processes (and to avoid misinterpretation) 50 to 80 test calculations for each column were performed (in total about 350 calculations).

The benefit of this study is that we can now ‘visualize’ and quantify the ongoing redox processes inside each column as a function of time  $t$  and distance  $x$ . Processes that are unseen in the experiments are become uncovered now. Please note that the measured data for the two N-species, nitrite and ammonium, are very sparse. This experimental information alone is insufficient to draw any picture of redox zonation. Only the combination of experiment and model calculation provides an adequate understanding of the complex dynamics (as it will be done in the next paragraph).

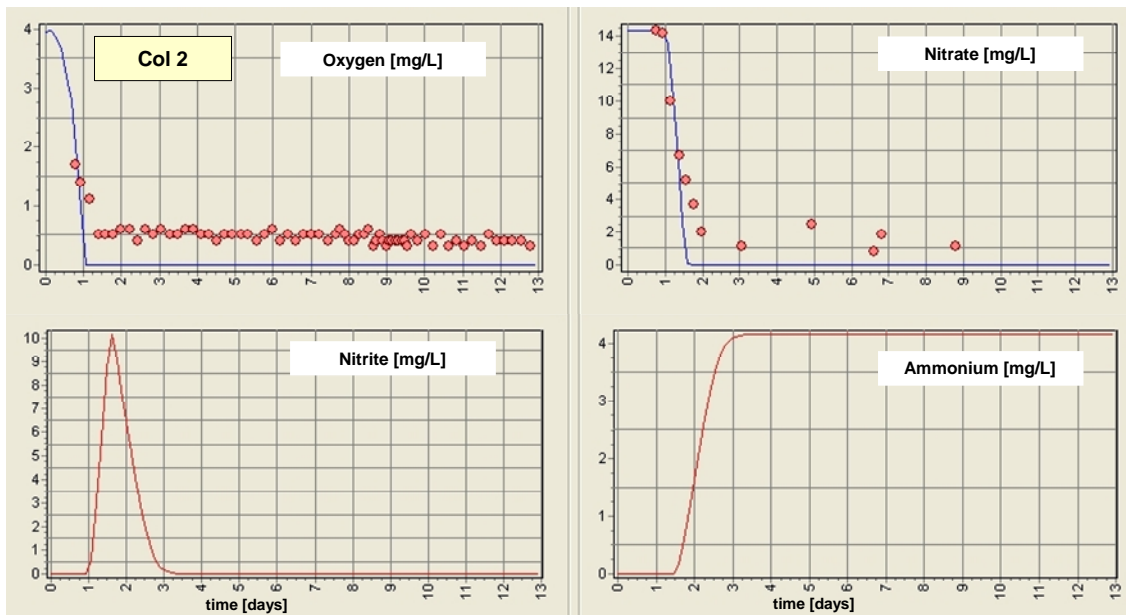


Fig. 4.7 Oxygen, nitrate, nitrite, and ammonium in the outflow solution of Col 2 as a function of time (model calculations and experiments; for nitrate and ammonium experimental data do not exist).

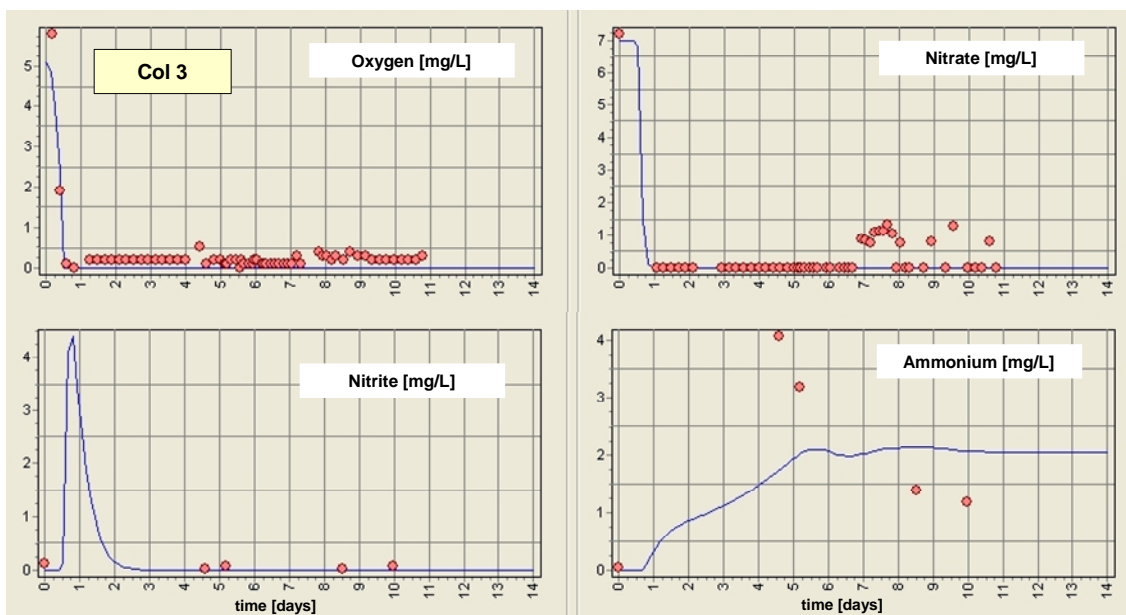
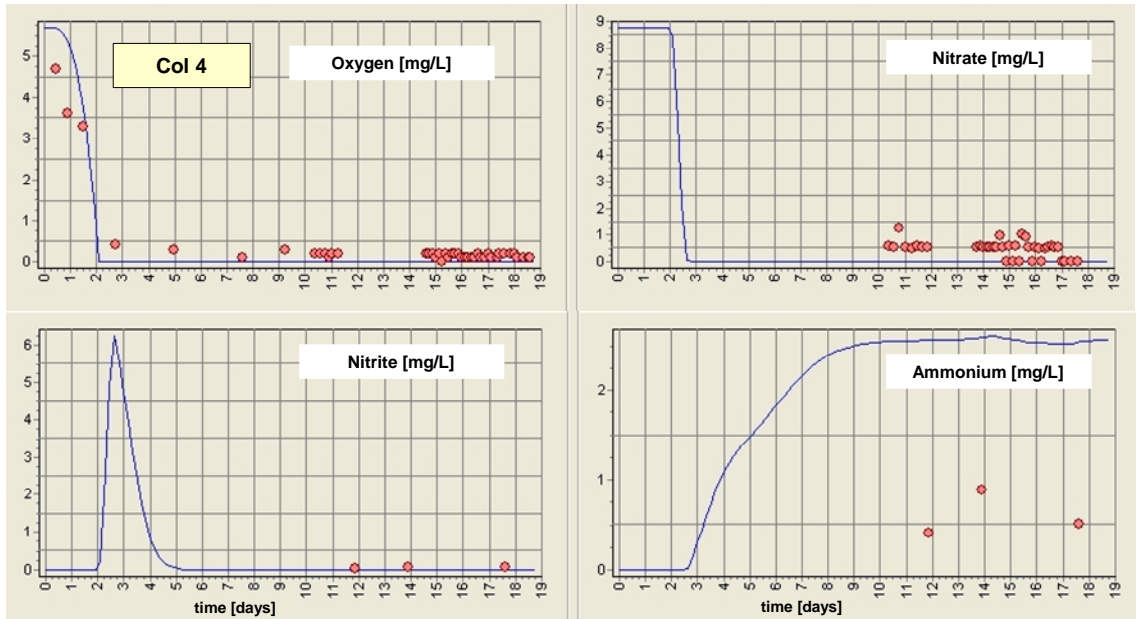
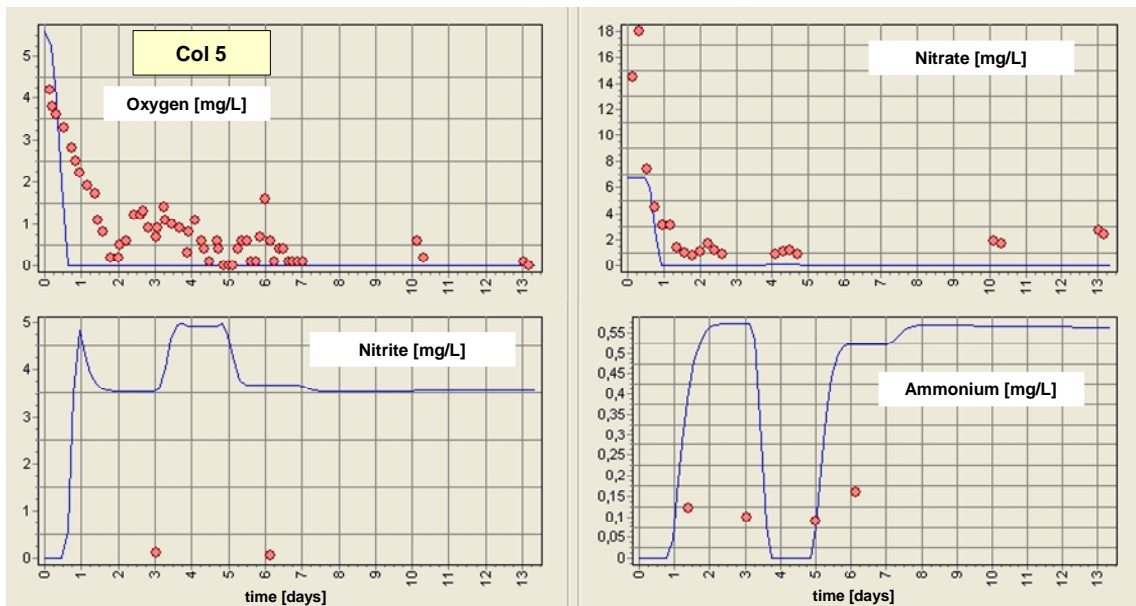


Fig. 4.8 Oxygen, nitrate, nitrite, and ammonium in the outflow solution of Col 3 as a function of time (model calculations and experiments).



**Fig. 4.9** Oxygen, nitrate, nitrite, and ammonium in the outflow solution of Col 4 as a function of time (model calculations and experiments).



**Fig. 4.10** Oxygen, nitrate, nitrite, and ammonium in the outflow solution of Col 5 as a function of time (model calculations and experiments).

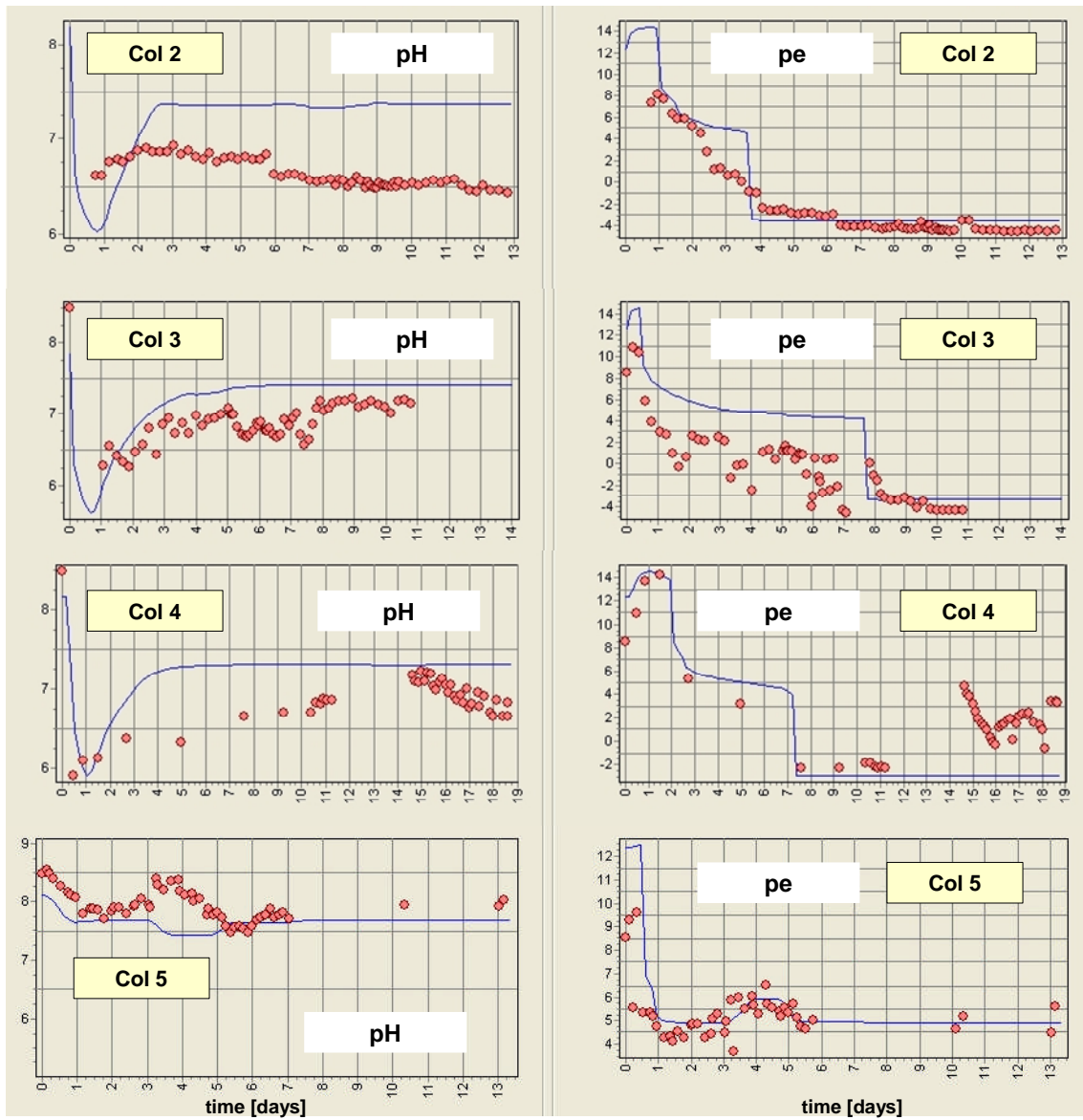


**Fig. 4.11** pH and pe values in the outflow solution of Col 2 to Col 5 as a function of time (model calculations and experiments).

## 4.5.2 Interpretation – Redox Zonation inside Columns

The dynamics of the ongoing redox processes in time and space is illustrated in Fig. 4.12 and Fig. 4.13. Fig. 4.12 shows the concentration of O<sub>2</sub> and three N species in the outflow solution of Col 3 as a function of time. Please note how oxygen, nitrate, nitrite, and ammonium seep out the column one after the other. Once O<sub>2</sub> is depleted nitrate transforms into nitrite; then nitrite transforms into ammonium so that after about 3 days ammonium remains as the only N-species in the outflow solution. The steady state is achieved after 7-8 days where the mass balance is fulfilled:

$$\text{inflow concentration of NO}_3^- = \text{outflow concentration of NH}_4^+ = 0.1 \text{ mM}$$

Ammonium, NH<sub>4</sub><sup>+</sup>, as the only cation of all four redox species is absorbed on the ion exchanger. Therefore, in contrast to the other three species with a sharp breakthrough, the ammonium curve is retarded (smoothed). The loading on the ion exchanger occurs during the first 5 days. After this time ammonium reaches the saturation value of 0.1 mM in the outflow.

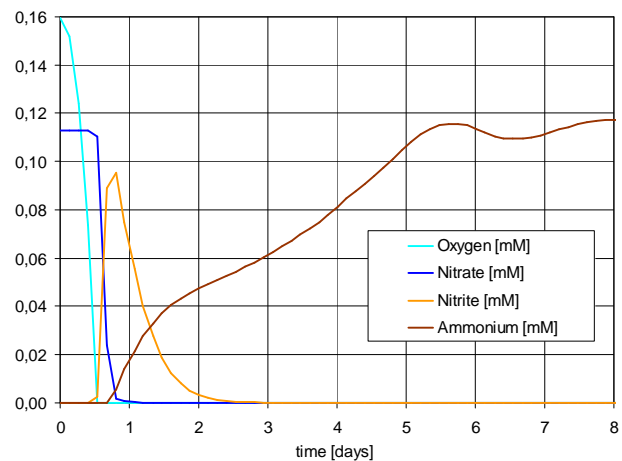


**Fig. 4.12** Oxygen, nitrate, nitrite, and ammonium in the outflow solution of Col 3 as a function of time.

**Redox Zonation.** The forming of redox zones inside Col 3 is shown in Fig. 4.13 at four different times. At the beginning (upper diagram) the column is filled with O<sub>2</sub>- and nitrate-rich water (no zonation). This oxidized water is injected into the column and maintains oxidizing conditions at the column inlet (first column cells near  $x \approx 0$ ). When time passes biodegradation establishes reductive condition inside the column (about 5 cm away from the entrance, and especially at the column outlet). After 20 hours (2<sup>nd</sup> diagram) nitrite is produced inside the column; after 45 hours (3<sup>rd</sup> diagram) ammonium appears. At the same time O<sub>2</sub> is depleted completely. The last diagram (after 70 hours) shows that the reductive conditions once established will prevail as a ‘steady state’ until the entire organic material is degraded (which, however, would require longer experimental time).

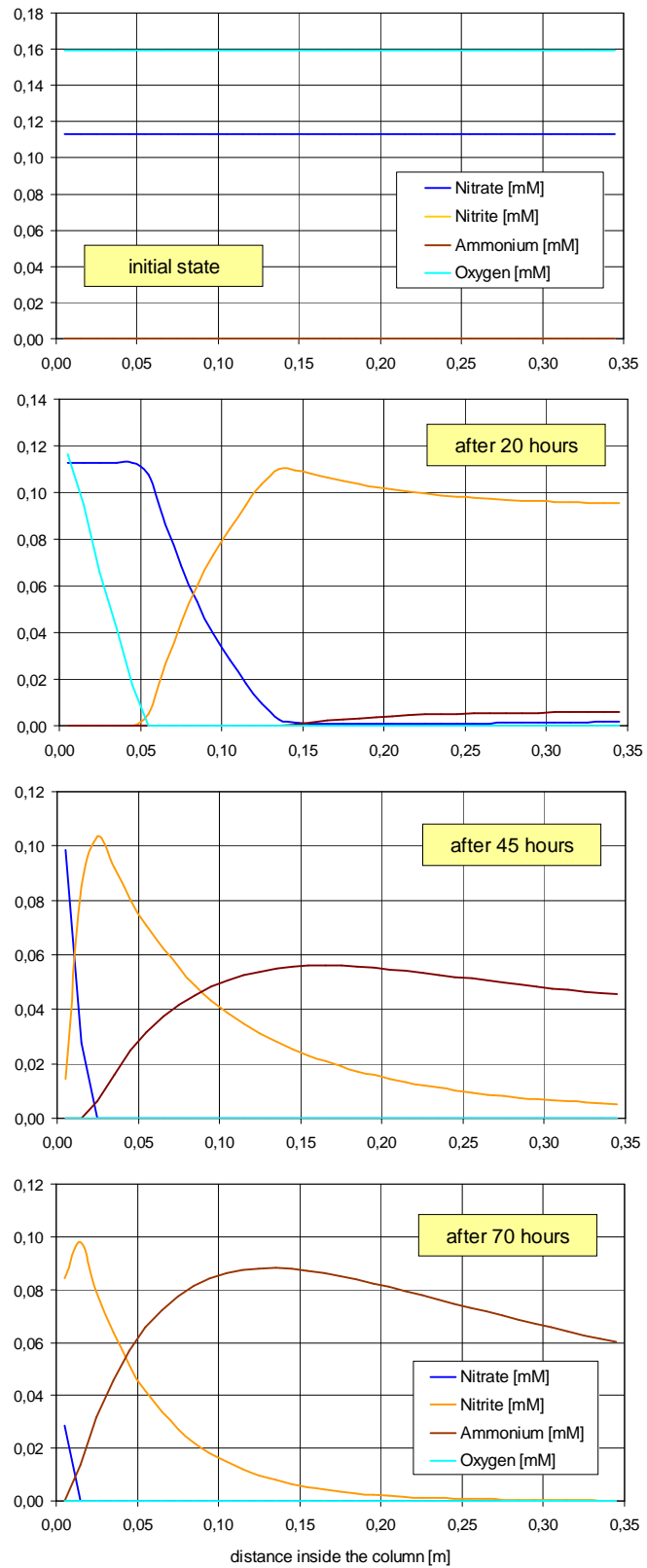
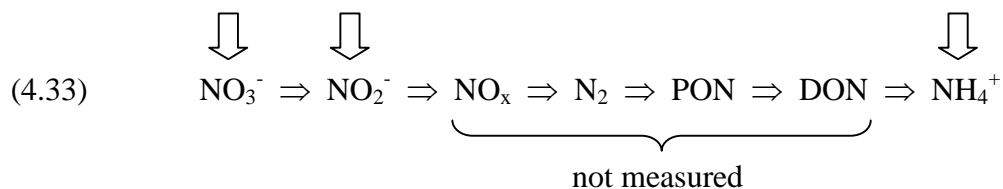


Fig. 4.13 Redox zonation within Col 3 at different times (initial state in upper diagram)

### 4.5.3 Limits and Benefits

**Limits.** The model represents a *first* approach to the complex branch of redox processes. Thus, we focused on three N species: nitrate, nitrite, and ammonium (the only concentrations that are measured):



The formation of N<sub>2</sub> gas is not considered yet. However, in contrast to bioreactors (as ‘open systems’) aquifer and columns represent ‘closed systems’ where gas formation is more or less constraint. The good description of both pe value *and* ammonium justify the chosen approach.

[Note: Probably two effects (not considered in the model) compensate each other: The formation of additional ammonium during degradation of organic matter and the depletion of ammonium due to escape of N<sub>2</sub>.]

**Model & Experiments.** The present WP 3 demonstrates a sound combination of ‘experiment’ and ‘theory’. Due to this combination we are able to reveal details about the redox system that we didn’t think beforehand (looking on raw data alone).

**Outlook.** Once a model is calibrate by *real* data it can be used as a predictive tool for scenario simulations:

- variation of flow velocity and other hydraulic/geometric parameters
- multi-layer systems with natural sediments and/or technical sand
- long-term experiments (≥ 3 month)
- larger columns (upscaling)
- column systems (including reactors)

The extension and upgrade of the model is an ongoing process (based on site- and project-specific data and knowledge). In this way, the model is ready to incorporate new aspects of geochemistry and geomicrobiology.



## 5 SUMMARY

The present report belongs to Work Package 3 “Redox Control and Optimization at AR Ponds” of the OXIRE2 project started in January 2010. Work Package 3 consists of two main parts and was performed in cooperation with TUB:

- Part I. Laboratory column experiments with special emphasis on sediment characteristics (by TUB)
- Part II Numerical modeling of the results of the TUB column experiments (by UIT; present report)

The present report focuses on the *geochemical* interpretation of the TUB column experiments. A reactive transport model TRN – based on the U.S.G.S. code PHREEQC – was used to simulate four column tests (Col 2, Col 3, Col 4, and Col 5). The study was performed in several steps, from the simplest to the most complicated one:

- hydraulics (advection & dispersion) in § 3.1
- cation exchange in § 3.2
- mineral phases (calcite kinetics) in § 3.3
- redox reactions and biodegradation in Chapter 4

The system is highly dynamic. The aim was to combine all these separate processes into a coherent whole that explains the formation of redox zones inside the columns (as a function of time and column depth).

**Hydraulics.** The study starts with the adjustment of the *hydraulic* and *geometric* parameter set for each column. This was done by fitting the breakthrough curve of bromide (resulting from added LiBr to the inflow solution). Whereas the anion Br<sup>-</sup> acts as perfect tracer the cation Li<sup>+</sup> undergoes *ion exchange*.

**Ion Exchange.** The breakthrough of Li<sup>+</sup> was used to extract the ion-exchange capacity CEC of the sediment. The deduced CEC of 20 meq/L agrees well with theoretical estimations for the sediment in Col 2 to Col 4. In Col 5, however, the sediment was pre-treated at 550 °C causing a temperature-driven artificial weathering which results in a smaller CEC of 5 meq/L.

Ion exchange is crucial to understand the behavior of other cations, especially K<sup>+</sup>, Mg<sup>+2</sup>, NH<sub>4</sub><sup>+</sup> (as well as the retardation of carbamazepine). K<sup>+</sup> as a non-reactive element is only influenced by ion exchange (like Li<sup>+</sup>). The good agreement between the calculated and observed concentrations in Fig. 3.5 reflects the quality of the ion-exchange model (where the time-dependent behavior of K<sup>+</sup> is caused solely by loading and deloading of the competing ions like Ca and Mg).

**Mineral Dissolution.** The only mineral that significantly influences the column system is *calcite*. The extraordinary role of calcite already becomes clear from the hydrochemistry of the inflow water from Lake Tegel. This water is super-saturated with calcite, what calls for a *kinetic* approach (instead of pure equilibrium thermodynamics). The calcite dissolution rate was adjusted to describe the outflow concentrations of Ca, DIC, and pH value.

**Redox Reactions.** Redox reactions are the central part of the present study. For this purpose a *biodegradation* model was established (and included into the reactive transport model). The biodegradation model bases on a combined approach of *enzyme kinetics* and thermodynamics. Whereas the degradation of organic matter in Eq. (4.8) is treated by enzyme kinetics the accompanied *electron transfer* and electron balance is controlled by thermodynamics (using PHREEQC). In PHREEQC all relevant redox reactions are considered *per se*; they are defined in the thermodynamic database (wateq4f) which contains a long list of reaction equations (stoichiometry) and log K values (equilibrium constants).

From the mathematical point of view, the redox system is highly *non-linear*. Just small changes of one single element concentration cause huge changes of the pe value. This effect is observable, for example, in the pe diagrams of Fig. 4.11. In this way, the numerical simulation of redox reactions belongs to the most complicated tasks in hydrochemistry. In order to understand the ongoing processes (and to avoid misinterpretation) 50 to 80 test calculations for each column were performed (in total about 350 calculations).

**Redox Zonation.** The benefit of the biodegradation model is that now we can quantify the ongoing redox processes inside each column as a function of time and column depth. Processes that are unseen in the experiments are become uncovered now, especially the transition from nitrate to nitrite to ammonium (despite the very sparse experimental data for nitrite and ammonium). In this case, only the combination of experiment *and* model calculation provides an adequate understanding of the complex dynamics (as shown in § 4.5.2).

**Outlook.** Once a model is calibrate by *real* data it can be used as a predictive tool for scenario simulations:

- variation of flow velocity and other hydraulic/geometric parameters
- multi-layer systems with natural sediments and/or technical sand
- long-term experiments ( $\geq 3$  month)
- larger columns (upscaling)
- column systems (including reactors)

The model is ready to incorporate new aspects of geochemistry and geomicrobiology.

## REFERENCES

- [AP05] Appelo C.A.J., D. Postma: *Geochemistry, Groundwater and Pollution*, Second Edition, CRC Press Taylor & Francis Group, Boca Raton, 2005
- [Br94] Brezonik, P.L.: *Chemical Kinetics and Process Dynamics in Aquatic Systems*, Lewis Publishers, Boca Raton: CRC Press LLC, 1994
- [DS97] Domenico P.A., F.W. Schwartz: *Physical and Chemical Hydrogeology*, John Wiley & Sons, Inc. New York 1997
- [KWB10] Reuleaux, M., G. Grützmacher: *Literature Study on Published Experience with Redox Control in Infiltration Ponds and other Subsurface Systems*, Kompetenz-Zentrum Berlin, Dec 2010
- [La87] Lasch, J.: *Enzymkinetik*, VEB Gustav Fischer Verlag, Jena 1987
- [MH93] Morel F.M.M., J.G. Hering: *Principles and Applications of Aquatic Chemistry*, John Wiley & Sons, New York 1993
- [Num03] Press W.H., S.A. Teukolsky, W.T. Vetterling, B.P. Flannery: *Numerical Recipes in C++ – The Art of Scientific Computing*, Second Edition, Cambridge University Press, 2003
- [Pa95] Panikov, N.S.: *Microbial Growth Kinetics*, Chapman & Hall, London 1995
- [PA99] Parkhurst David L, C.A.J Appelo: *User's guide to PHREEQC (version 2) – a computer program for speciation, batch-reaction, one-dimensional transport, and inverse geochemical calculations*, Water-Resources Investigation Report 99-4259, Denver, Colorado 1999
- [Sch89] Schellenberger, A.: *Enzymkatalyse*, VEB Gustav Fischer Verlag, Jena 1989
- [TUB11] Scheytt, T., B. Müller: *Laboratory Column Experiments on Options for Redox Control in Air Infiltration Ponds – OXIREDD 2 WP3, Deliverable D3.4 – Part I*, TU Berlin, Feb 2011





**UMWELTLEISTUNGEN**



---

# Appendix

---



# A REACTIVE TRANSPORT

## A.1 Definition of the System

### A.1.1 Aqueous and Mineral Phases

The reactive transport model combines transport with reactions (chemical equilibrium and kinetics). The reaction module describes the mass transfer of species  $i$  between several phases:

- |       |                     |                           |
|-------|---------------------|---------------------------|
| (A.1) | mobile water:       | $m_i^W = c_i^W \cdot V_W$ |
| (A.2) | stagnant water:     | $m_i^P = c_i^P \cdot V_P$ |
| (A.3) | secondary minerals: | $m_i^S$                   |
| (A.4) | ion exchange:       | $m_i^Y$                   |
| (A.5) | primary minerals:   | $m_i^R$                   |

Here,  $m_i$  denotes the mass (amount in moles),  $c_i$  the concentration (in mol/L), and  $V$  the water volume.

The distinction between two water phases (mobile and stagnant) is a key feature of the so-called ‘dual-porosity approach’. The mass transfer between all phases is depicted in Fig. A.1.

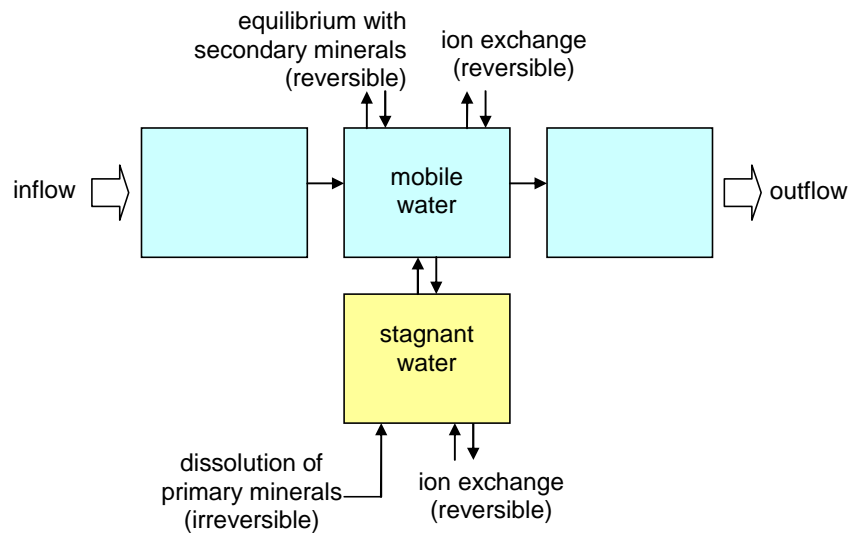


**Fig. A.1** Interplay of all processes within one cell of a 1D-column (dual porosity approach)

The reversible reactions (mineral phase equilibrium and ion exchange) are calculated by the thermodynamic code PHREEQC [PA99]; irreversible reactions (mineral dissolution) are based on a kinetic approach.

## A.1.2 Main Equations

**Dual Porosity.** The complete system for the dual-porosity approach is described by a set of differential equations (stoichiometric coefficients are omitted in order to keep the notation straight):

$$(A.6) \quad \frac{\partial m_i^W}{\partial t} = -v \frac{\partial m_i^W}{\partial X} + D_L \frac{\partial^2 m_i^W}{\partial X^2} + \alpha V_P (c_i^P - c_i^W) - J_{W \leftrightarrow S}$$

$$(A.7) \quad \frac{dm_i^P}{dt} = -\alpha V_P (c_i^P - c_i^W) - J_{P \leftrightarrow Y} + J_{\text{reac}}$$

$$(A.8) \quad \frac{dm_i^S}{dt} = J_{W \leftrightarrow S} \quad (\text{thermodynamic model})$$

$$(A.9) \quad \frac{dm_i^Y}{dt} = J_{P \leftrightarrow Y} \quad (\text{thermodynamic model})$$

$$(A.10) \quad \frac{dm_i^R}{dt} = -J_{\text{reac}} \quad (\text{kinetic model})$$

The first two terms in Eq. (A.6) describe advection (with velocity  $v$ ) and dispersion (with the longitudinal dispersion coefficient  $D_L$ ). The exchange between both water phases is controlled by the rate  $\alpha$  (third term). The ‘rates’  $J_{W \leftrightarrow S}$  and  $J_{P \leftrightarrow Y}$  symbolize the precipitation/dissolution of secondary minerals and the ion exchange; both are calculated by PHREEQC. Finally, for the primary mineral dissolution rate  $J_{\text{reac}}$  several kinetic approaches are possible, for example:

$$(A.11) \quad J_{\text{reac}} = r \cdot \left( \frac{m}{m_0} \right) \quad (\text{first-order kinetics})$$

$$(A.12) \quad J_{\text{reac}} = r \cdot \left( \frac{m}{m_0} \right) \cdot (1 - 10^{SI})$$

$$(A.13) \quad J_{\text{reac}} = r \cdot \left( \frac{m}{m_0} \right) \cdot 10^{-b \cdot \text{pH}} \cdot (1 - 10^{SI})$$

$$(A.14) \quad J_{\text{reac}} = \text{enzyme kinetics} \quad (\text{mixed-order kinetics})$$

and other sophisticated kinetics (such as pyrite oxidation).

**Single Porosity.** In the case of single-porosity approach the above set of differential equations reduces to:

$$(A.15) \quad \frac{\partial m_i^W}{\partial t} = -v \frac{\partial m_i^W}{\partial X} + D_L \frac{\partial^2 m_i^W}{\partial X^2} - J_{W \leftrightarrow S} - J_{W \leftrightarrow X} + J_{\text{reac}}$$

$$(A.16) \quad \frac{dm_i^S}{dt} = J_{W \leftrightarrow S} \quad (\text{thermodynamic model})$$

$$(A.17) \quad \frac{dm_i^Y}{dt} = J_{W \leftrightarrow Y} \quad (\text{thermodynamic model})$$

$$(A.18) \quad \frac{dm_i^R}{dt} = -J_{\text{reac}} \quad (\text{kinetic model})$$

**Dual-Porosity Mass Transfer.** The diffusion-like mass transfer between stagnant and mobile water is controlled by the rate parameter  $\alpha$  in Eqs. (A.6) and (A.7). For the extreme case  $\alpha = 0$  there is no interaction at all; otherwise, for  $\alpha = \infty$  the double porosity approach converges to the single porosity model.

An estimate of  $\alpha$  is given by VAN GENUCHTEN's approach [VG85]

$$(A.19) \quad \alpha = \frac{D \cdot \varepsilon_{\text{res}}}{(a \cdot f_{s \rightarrow l})^2}$$

where  $D$  is the diffusion coefficient (in the order of  $10^{-9} \text{ m}^2/\text{s}$ ),  $a$  is the particle radius, and  $f_{s \rightarrow l} = 0.2$  the shape factor.

**Dispersivity.** The relation between the dispersion coefficient  $D_L$  and the longitudinal dispersivity  $\alpha_L$  is given in Eq. (A.29).

## A.2 Transport Phenomena

### A.2.1 Advection in a Homogeneous System

For systems with fluid motion, mass transport is due to both advection and hydrodynamic dispersion, which are described by the first two terms in Eq. (A.6). The advection-dispersion equation,

$$(A.20) \quad \frac{\partial c_i}{\partial t} = -v \frac{\partial c_i}{\partial x} + D_L \frac{\partial^2 c_i}{\partial x^2}$$

is the workhorse for modeling studies in groundwater contamination [DS97].

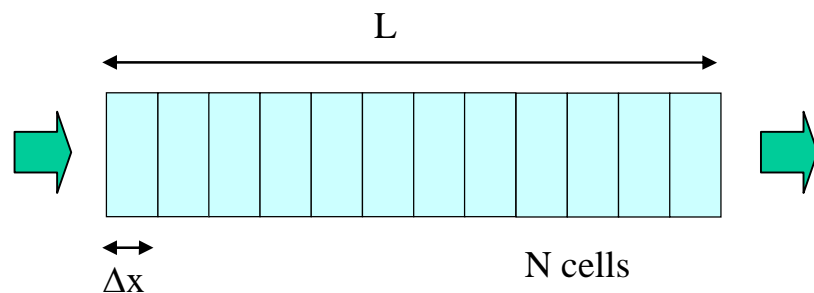


**Fig. A.2** Discretization of an homogeneous 1D-system into  $N$  cells

**Homogeneous System.** In order to discuss the advection we consider a homogeneous 1D-system of total length  $L$ , cross section  $A$ , and porosity  $\varepsilon$ . According to a spatial discretization the system will be decomposed into  $N$  cells of equidistant length  $\Delta x$  (see Fig. A.2), whereas

$$(A.21) \quad \Delta x = \frac{L}{N} \quad (\text{cell length})$$

In the homogeneous system all cells have the same pore volume

$$(A.22) \quad \Delta V_{\text{pore}} = \varepsilon A \cdot \Delta x$$

Given the volumetric flow  $Q$  as the constant inflow rate, the timestep width can be determined by

$$(A.23) \quad \Delta t = \frac{\Delta V_{\text{pore}}}{Q} = \frac{\varepsilon A \Delta x}{Q}$$

The relation between pore velocity  $v$  and inflow rate  $Q$  is given by

$$(A.24) \quad v = \frac{Q}{\varepsilon A} = \frac{\Delta x}{\Delta t}$$

Using this relationship between time and distance discretization,  $\Delta t = \Delta x/v$ , numerical dispersion is minimized [AP05]. This is a great advantage of the applied procedure. Thus, in case of pure advection we simply move along, pouring at every time step concentrations from one cell into the next one. Fronts move neatly and remain sharp. Such sharpness is blurred when front transfer and grid boundaries do not correspond (i.e. when  $\Delta t \neq \Delta x/v$ ). In this case the mixing of old and new concentrations in a cell leads to gradual smoothing of transitions (which is called *numerical* dispersion). In conclusion, applying rigorously Eq. (A.24) our model becomes free of numerical dispersion. (A quite similar approach is used in the advection procedure of PHREEQC [PA99].)

## A.2.2 Advection in a Heterogeneous System

In practice, the mass transport often takes place in heterogeneous systems where the water flow transverses several layers (for example a passage from sandy aquifers to dense sediments and vice versa). To account for this situation the system will be divided into several homogeneous segments (compartments, layers). Each segment  $K$  is again subdivided into  $N_K$  cells. Fig. A.3 shows an example of an inhomogeneous system decomposed in three homogeneous segments (layers). In the model, the number of segments/layers, as well as the number of cells, is unlimited.

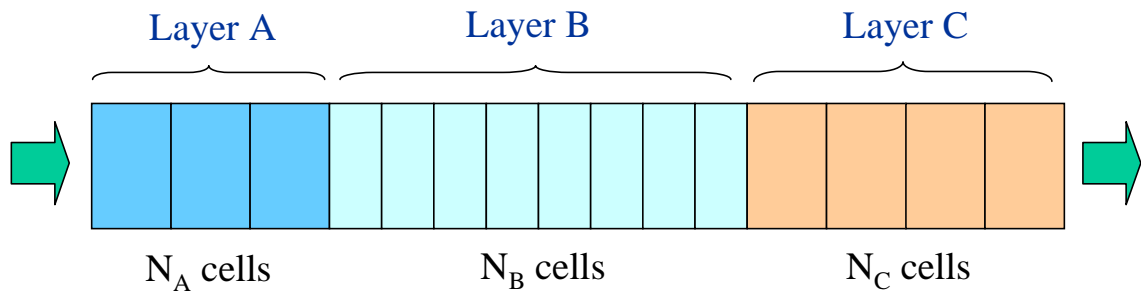


Fig. A.3 Decomposition of an inhomogeneous system into three homogeneous segments (layers)

To employ the advantages of the model described in § A.2.1 (i.e. a model without numerical dispersion), the cell structure of the compartments should fulfill the condition that all cells in the system have the same pore volume:

$$(A.25) \quad \Delta V_p = \text{const} = \varepsilon_A A \Delta x_A = \varepsilon_B A \Delta x_B = \dots$$

Thus, given a constant inflow rate  $Q$ , at every time step

$$(A.26) \quad \Delta t = \frac{\Delta V_p}{Q} = \frac{\varepsilon A_K \Delta x_K}{Q} = \text{const} \quad (\text{for all layers } K)$$

the pore volume  $\Delta V_p$  of cell  $n$  is shifted entirely to the next cell  $n+1$ . In consequence of Eq. (A.25) the chosen cell length  $\Delta x$  depends on the porosity  $\varepsilon$ . In other words, within a layer of a given porosity  $\varepsilon_1$  all cells obey the same cell lengths  $\Delta x_1$ , and this cell length differs from any other layer of porosity  $\varepsilon_2$ . Further on, whereas  $Q$  is constant in the whole system the pore velocity  $v$  differs from layer to layer:

$$(A.27) \quad v_K = \frac{Q}{\varepsilon_K A} = \frac{\Delta x_K}{\Delta t} \neq \text{const}$$

The total number of cells of a heterogeneous system is

$$(A.28) \quad N = N_A + N_B + \dots = \frac{L_A}{\Delta x_A} + \frac{L_B}{\Delta x_B} + \dots$$

### A.2.3 Dispersion

The coefficient of hydrodynamic dispersion,  $D_L$ , incorporates the combined effects of diffusion and mechanical dispersion

$$(A.29) \quad D_L = D_e + \alpha_L v$$

Dispersivity  $\alpha_L$  (in cm or m) represents the spreading of a solute over a given length of flow. If there is no water flow at all,  $v = 0$ , mechanical dispersion vanishes, i.e., the hydrodynamic dispersion reduces to diffusion,  $D_L = D_e$ .

The process of molecular diffusion is slower in porous media than in open water because ions must follow the tortuous flow paths [DS97]. To account for this an effective molecular diffusion coefficient is used

$$(A.30) \quad D_e = wD = \frac{D}{\tau} \quad \text{with} \quad w = 0.01 \dots 0.5$$

Here, the meaning of the symbols is:

$D_L$	hydrodynamic dispersion coefficient	$[L^2/T]$
$D_e$	effective diffusion coefficient	$[L^2/T]$
$D$	molecular diffusion coefficient	$[L^2/T]$
$\alpha_L$	longitudinal dispersivity	$[L]$
$w$	empirical coefficient	[unitless]
$\tau$	tortuosity	[unitless]

The usual assumption is that the pore velocity  $v$  and the dispersion coefficient does not dependent on the type of solute species.

**Numerics.** Numerical instabilities (oscillations) in the calculation of dispersion are eliminated with the constraint [PA99]:

$$(A.31) \quad \Delta t_D \leq \frac{\Delta x}{3D_L} \quad (\text{dispersion time step})$$

This quantity should be compared with the advection time step defined in § A.2.1:

$$(A.32) \quad \Delta t = \frac{\Delta x}{v} \quad (\text{advection time step})$$

The meaning of Eq. (A.31) is explained easily: Dispersive transport is essentially mixing of cells. The restriction is that never more solution is mixed out of a cell than stays behind. Thus, if  $\Delta t_D$  is  $n_D$  times smaller than  $\Delta t$ ,

$$(A.33) \quad \Delta t_D = \frac{\Delta t}{n_D}$$

then,  $n$  mixes at every time step  $\Delta t$  will be performed automatically .

## A.2.4 Numerical Model versus Analytical Solution

We consider the general expression of a transport equation with retardation (due to sorption) and first-order kinetics

$$(A.34) \quad R \frac{\partial c}{\partial t} = -v \frac{\partial c}{\partial x} + D \frac{\partial^2 c}{\partial x^2} - \lambda c$$

with  $\lambda$  as degradation constant and where the retardation factor is defined as

$$(A.35) \quad R = 1 + \frac{\rho_b}{\phi} K_d$$

The initial and boundary conditions are given by

$$(A.36) \quad \begin{aligned} c &= 0 \quad \text{for } t = 0, \quad x > 0 \\ c &= c_0 \quad \text{for } x = 0, \quad t > 0 \\ c &= 0 \quad \text{for } x = \infty, \quad t > 0 \end{aligned}$$

The initial condition (first line) states that at all points have at time  $t = 0$  zero concentration. The first boundary condition (second line) states that at  $x = 0$ , for all time  $t$ , the concentration is  $c_0$  (that is, a continuous source). The analytical solution is:

$$(A.37) \quad c(x, t) = \frac{c_0}{2} \left\{ \exp \frac{x(v-w)}{2D} \cdot \operatorname{erfc} \frac{Rx-wt}{\sqrt{4DRt}} + \exp \frac{x(v+w)}{2D} \cdot \operatorname{erfc} \frac{Rx+wt}{\sqrt{4DRt}} \right\}$$

with the abbreviation

$$(A.38) \quad w = \sqrt{v^2 + 4DR\lambda}$$

and the complementary error function

$$(A.39) \quad \operatorname{erfc} x = \frac{2}{\sqrt{\pi}} \int_x^{\infty} \exp(-t^2) dt$$

If there is no retardation,  $R = 0$ , and no degradation,  $\lambda = 0$ , we have  $w = v$ . In this special case Eq. (A.37) reduces to the so-called Ogata-Banks equation:

$$(A.40) \quad c(x, t) = \frac{c_0}{2} \left\{ \operatorname{erfc} \frac{x-vt}{\sqrt{4Dt}} + \exp \frac{xv}{D} \cdot \operatorname{erfc} \frac{x+vt}{\sqrt{4Dt}} \right\}$$

**Numerical Test.** An analytical solution of the ADR equation only exists for some special cases (like homogeneous flow tube, no higher order kinetics etc.) with the initial and boundary conditions defined in Eq. (A.36). In the following, we consider 3 special cases of an 1-dimensional plug flow:

A	transport with small dispersion	$\alpha_L = 0.005 \text{ m}$
B	transport with medium dispersion	$\alpha_L = 0.05 \text{ m}$
C	transport with large dispersion	$\alpha_L = 0.10 \text{ m}$

The size of the flow tube and the hydraulic parameters for all 3 cases are given by:

total length	$L = 1.0 \text{ m}$
number of cells	$N = 40$
cell length	$\Delta x = L/N = 0.025 \text{ m}$
porosity	$\varepsilon = 0.2$
flow velocity	$v = 0.2 \text{ m/day}$
time step	$\Delta t = \Delta x/v = 3 \text{ h}$

Given a flow tube or column of diameter  $d = 42 \text{ mm}$ , the cross section area is  $A = (\pi/4)d^2 = 1.38 \cdot 10^{-3} \text{ m}^2$ . This correspond to

total pore volume	$V_P = \varepsilon AL = 2.76 \cdot 10^{-5} \text{ m}^3$
pore volume of a cell	$\Delta V_P = V_P/N = 0.69 \cdot 10^{-6} \text{ m}^3$
volumetric flux	$Q = \Delta V_P/\Delta t = 0.23 \text{ mL/h}$

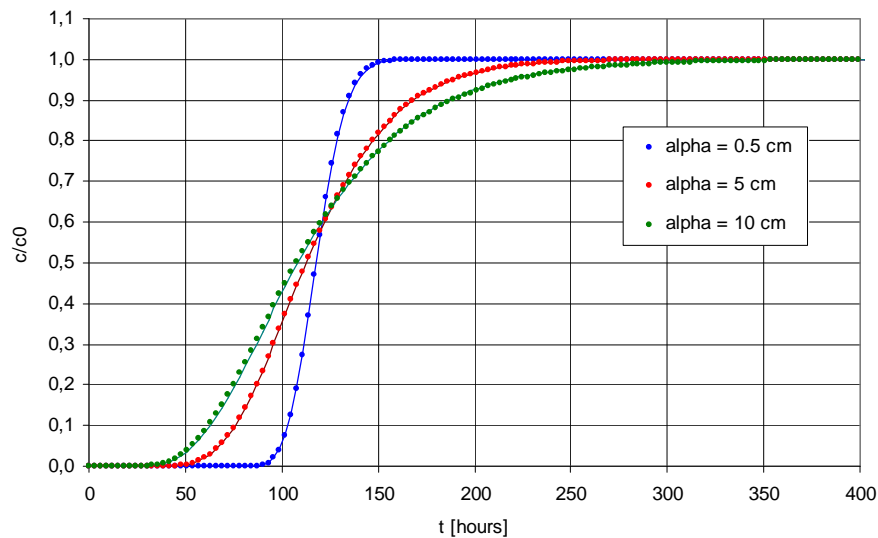


**Fig. A.4** Comparison of the numerical model (circles) with analytical solutions (lines) for three dispersivities  $\alpha_L$

The time needed for one pore-volume exchange is  $T_P = V_P/Q = 120 \text{ h}$ . The simulation is  $t_E = 400 \text{ h}$  which correspond to 3.33 pore-volume exchanges.

The comparison between the numerical model and the analytical solution, i.e. Eq. (A.37), is shown in Fig. A.4. In all 3 cases the numerical model agrees with the exact solution.

### A.3 The Software

The software was written in the object oriented programming (OOP) language C++. The program consists of a clearly arranged user interface (see Fig. A.1) as well as visualization tools that present all results in form of diagrams and tables (see Fig. A.3). The simulation progress and the actual results can be observed by ‘online graphics’ (see Fig. A.2).

**Software Design.** In the philosophy of OOP, the model was build with a modular design that consists of a main program and “packages”. The packages are groups of independent subroutines that carry out specific simulation tasks such as transport, dispersion, sorption, kinetics, and chemical equilibrium calculations with PHREEQC. This modular design is useful in several respects. First, it provides a logical basis for organizing the actual code with similar program elements or functions grouped together. Second, such a structure facilitates the integration of new packages in order to enhance the code’s capabilities.

**Code Capabilities.** The program differs in several items from other existing reactive transport models. One of them is the special treatment of transport phenomena (advection without numerical dispersion, dispersion with interlacing time steps etc.).

Another advantage is the direct link between transport and hydrochemistry due to the inclusion of PHREEQC code with its thermodynamic database. It allows the consistent calculation of pH, of CO<sub>2</sub> equilibrium with HCO<sub>3</sub><sup>-</sup> and CO<sub>3</sub><sup>-2</sup> and, especially, the tricky redox reactions. In general, PHREEQC is characterized by:

- the number of chemical species (anions, cations, etc.) in aqueous solutions is unlimited
- the number of mineral phases is unlimited (thermodynamic database is extendable)
- complexation and speciation using activity models (DEBYE-HÜCKEL etc.)
- equilibrium with mineral phases (precipitation and dissolution)
- equilibrium with gas phases (open and closed systems)
- ion exchange

Finally, the numerical model is embedded in a comfortable graphical user interface (GUI). The model data (input and output) will be displayed in various diagrams and tables. The offline graphic allows the direct comparison of different runs (scenarios).

**Mass Balance.** During computation mass balance is checked in each timestep.

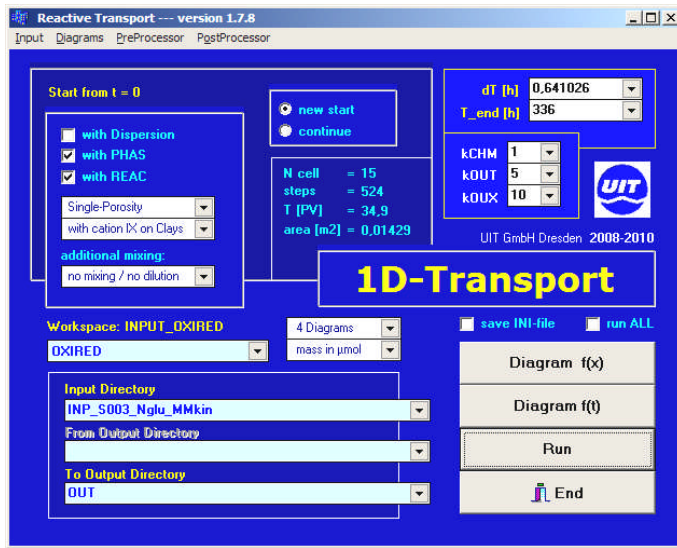


Fig. A.1 Main window of Reactive Transport Model TRN

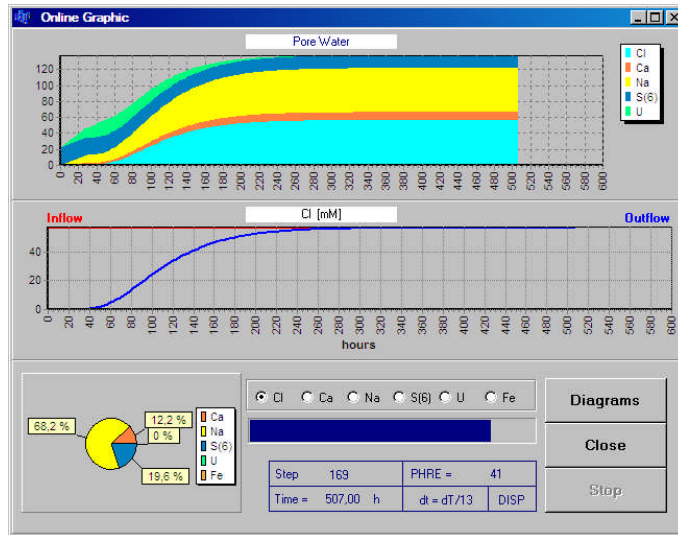


Fig. A.2 Online-graphic showing the inflow and outflow concentrations

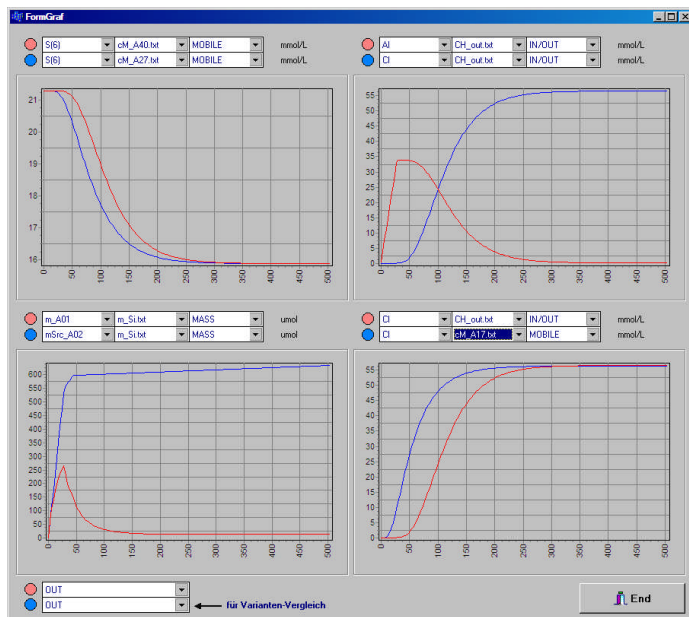
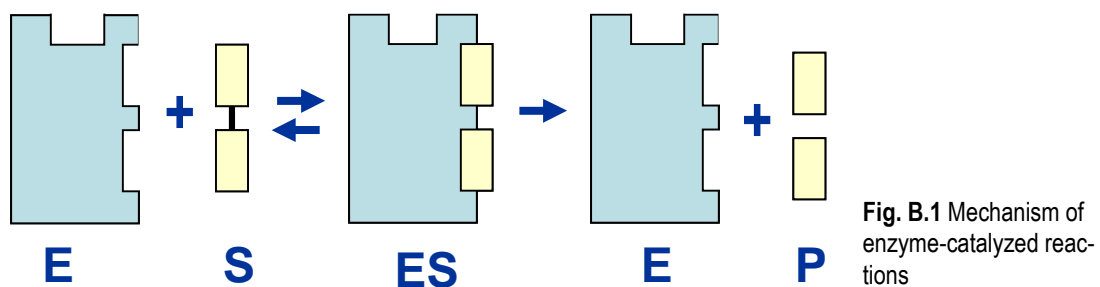


Fig. A.3 The complete output is visualized in diagrams

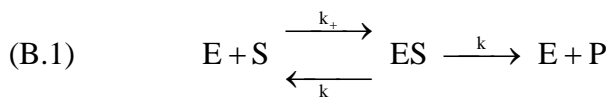
## B ENZYME KINETICS

### B.1 Michaelis-Menten Equation

The study of enzyme kinetics started at the turn of the century. It was found that (i) enzymes were true catalysts (being regenerated after each reaction event) and (ii) that catalysis occurred via the formation of enzyme-substrate complexes ES. A fundamental step forward was made 1913 by MICHAELIS and MENTEN who advanced a technique for measuring initial reaction rates under fully controlled conditions (by using a buffer to maintain constant pH) and who derived the basic equation of enzyme kinetics. This equation has been confirmed by numerous experiments over a period of more than 80 years. However, there are several deviations from the simple MICHAELIS-MENTEN kinetics, occurring if additional phenomena take place, like inhibition and inactivation of enzymes (see § B.2).



The simplest mechanism for enzyme-catalyzed reactions is (see Fig. B.1):



E represents the enzyme, S the substrate, P the product, and ES the enzyme-substrate complex. Concentrations in units  $M/L^3$  will be denoted by square brackets: [E], [S], [P], [ES]. In this notation, the total enzyme concentration,  $[E_T]$ , is defined by

$$(B.2) \quad [E_T] = [E] + [ES] \quad \text{material balance (enzyme balance)}$$

In Eq. (B.1) there are 3 transition rates:  $k$  and  $k_-$  are first-order constants with units  $T^{-1}$ ; the active complex formation rate  $k_+$  is a second order constant with units  $ML^{-3}T^{-1}$ . Applying the

$$(B.3) \quad \text{steady-state approximation:} \quad \frac{d[ES]}{dt} = 0$$

the rate of product formation can be derived:

$$(B.4) \quad \frac{d[P]}{dt} = -\frac{d[S]}{dt} = \frac{k[E_T][S]}{K_s + [S]}$$

This is the well known MICHAELIS-MENTEN equation where

$$(B.5) \quad K_s = \frac{k_- + k}{k_+} \quad (\text{BRIGGS \& HALDANE})$$

Usually, the product of  $k$  and  $[E_T]$  is lumped into a single parameter  $v_{\max}$ , which is called the maximum rate or maximum reaction velocity:

$$(B.6) \quad v_{\max} = k[E_T]$$

$K_s$  is known as the half saturation constant measured in concentration units  $M/L^3$ . Here, ‘half’ means if  $[S] = K_s$ , the formation rate becomes  $d[P]/dt = \frac{1}{2} v_{\max}$ .

The MICHAELIS-MENTEN equation contains two parameters:  $K_s$  and  $v_{\max}$ . There are several (graphical) approaches to estimate these parameters from batch degradation tests. Limiting conditions for this type of kinetics are listed at the end of this Section.

**Equilibrium Approach.** Equation (B.4) in combination with Eq. (B.5) was derived first by BRIGGS and HALDANE in 1925. In the special case of  $k_- \gg k$ , however, Eq. (B.5) simplifies to

$$(B.7) \quad K_s = \frac{k_- + k}{k_+} \xrightarrow{k_- \gg k} \frac{k_-}{k_+}$$

which was originally formulated by MICHAELIS and MENTEN in 1913. The meaning of this assumption is that the formation of the active complex in Eq. (B.1) is much faster than the product formation,  $ES \rightarrow E + P$ . If this assumption is valid, a pseudo-equilibrium exists between the substrate and the enzyme that can be expressed by the law of mass action

$$(B.8) \quad K_s = \frac{k_-}{k_+} = \frac{[E][S]}{[ES]} \quad (\text{MICHAELIS and MENTEN})$$

Here  $K_s$  acts as a dissociation constant of the ES-complex. In this approach, the substrate and the enzyme stay in equilibrium with each other while the substrate is being consumed. (Note: The equilibrium assumption and the steady-state approximation in Eq. (B.3) are quite different things; the first one is more restrictive.)

**Order of Kinetics.** The MICHAELIS-MENTEN equation (B.4) is plotted in Fig. B.2. This equation represents ‘kinetics of mixed order’ (comprising zero- and first-order kinetics). For high substrate concentrations it is of zero order; for small substrate concentration it is of first order:

$$(B.9) \quad [S] \gg K_s \quad \Rightarrow \quad d[S]/dt = -k[E_T] = \text{const}$$

$$(B.10) \quad [S] \ll K_s \quad \Rightarrow \quad d[S]/dt = -\lambda[S] \quad \text{with} \quad \lambda = k[E_T]/K_s$$

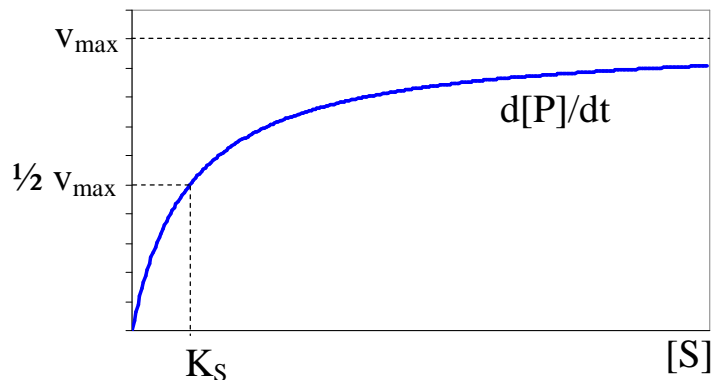


Fig. B.2 Plot of MICHAELIS-MENTEN equation

**Range of Validity.** The application of the MICHAELIS-MENTEN equation requires several preconditions [Br94]:

1. The reaction must involve a single substrate only (or the concentration of additional substrates must stay constant).
2. Because the reverse reaction ( $P + S \rightarrow ES$ ) is ignored in Eq. (B.1), *initial* velocities (= extrapolated values of  $d[S]/dt$  at  $t = 0$ ) must be measured at varying initial substrate concentrations  $[S_0]$ .
3. The concentration of the enzyme must be constant.
4.  $[E_0]$  must be much smaller than  $[S_0]$ ; otherwise it is not possible to apply the steady-state condition in Eq. (B.3).
5. Environmental conditions must be constant (temperature, pH, ionic strength).

## B.2 Enzyme Inhibition – HALDANE Equation

Inhibitors are compounds that bind to free enzymes rendering it unusable. Several kinds of inhibitor mechanisms exist. Three major classes of (product) inhibitors are:

- *competitive inhibition*, in which the inhibitor H and substrate S compete for the same reactive site on the enzyme (the alternative substrate H is chemically similar to the substrate)
- *self-inhibition*, in which high concentrations of substrate S inhibit the product formation. In this case, reaction rates reach a maximum at some intermediate  $[S]$  and then decline as  $[S]$  increases. This behavior is described by the so-called HALDANE formula.

- *non-competitive inhibition*, in which the inhibitor G and the substrate S may both be bound to the enzyme. The enzyme-substrate-inhibitor complex cannot form products.

Self-inhibition (also called substrate inhibition) is a special case of *uncompetitive inhibition*, in which the inhibitor binds to the enzyme-substrate complex, rather than to the free enzyme.

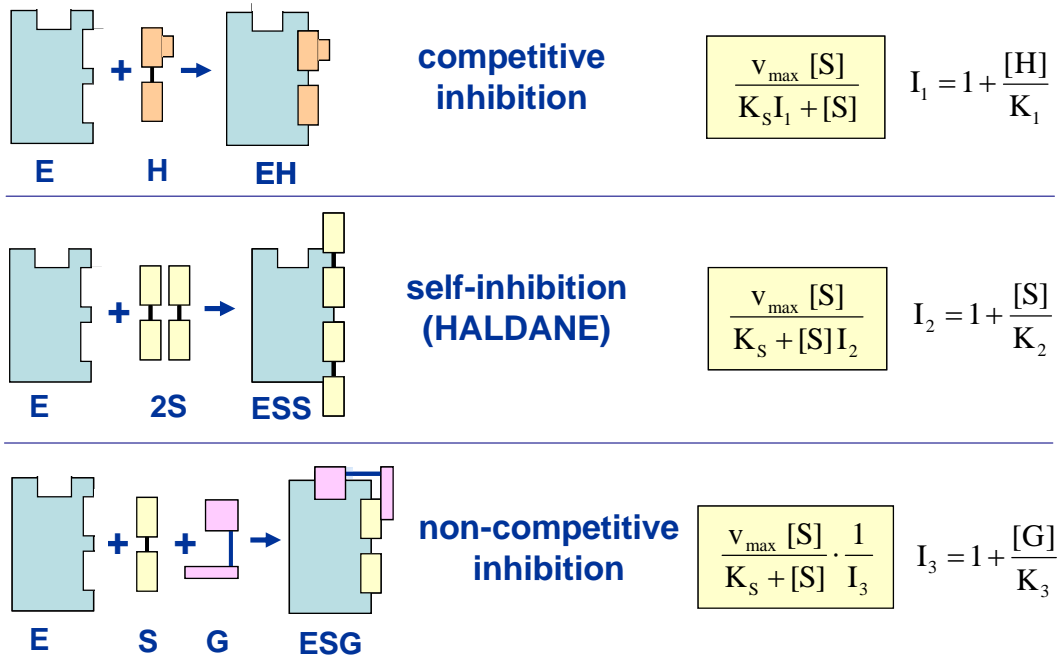


Fig. B.3 Three types of inhibitor mechanisms

The three types of inhibitor mechanisms are depicted in Fig. B.3. The corresponding inhibition-extended MICHAELIS-MENTEN equations are:

$$(B.11) \quad \frac{d[S]}{dt} = -\frac{v_{\max} [S]}{K_S I_1 + [S]} \quad \text{with} \quad I_1 = 1 + \frac{[H]}{K_1}$$

$$(B.12) \quad \frac{d[S]}{dt} = -\frac{v_{\max} [S]}{K_S + [S] I_2} \quad \text{with} \quad I_2 = 1 + \frac{[S]}{K_{SS}}$$

$$(B.13) \quad \frac{d[S]}{dt} = -\frac{v_{\max} [S]}{K_S + [S]} \cdot \frac{1}{I_3} \quad \text{with} \quad I_3 = 1 + \frac{[G]}{K_G}$$

It is quite easy to combine all three inhibition types and incorporate them into a single expression:

$$(B.14) \quad \frac{d[S]}{dt} = -\frac{v_{\max} [S]}{K_S I + [S] + [S]^2 / K_{SS}} \cdot \frac{K_G}{K_G + [G]}$$

Here the competitive-inhibition term

$$(B.15) \quad I = 1 + \sum_{j \neq S} \frac{[j]}{K_j^{\text{inh}}}$$

includes several alternate substrates [j]. The product in Eq. (B.15) runs over all inhibitors [j] excluding the ‘self-inhibitor’ S. (In case of reductive degradation dissolved oxygen is a non-competitive inhibitor: [G] = [O<sub>2</sub>], K<sub>G</sub> = K<sub>O<sub>2</sub></sub>.)

Once again, if there are neither competitive nor non-competitive inhibitors, [j] = 0 and [G] = 0, Eq. (B.14) reduces to the HALDANE equation:

$$(B.16) \quad \frac{d[S]}{dt} = - \frac{v_{\text{max}} [S]}{K_s + [S] + [S]^2 / K_{SS}} \quad (\text{HALDANE equation})$$

which is equivalent to Eq. (B.12). Here, K<sub>SS</sub> is the HALDANE parameter.

**Allosteric Inhibition.** So far, only conventional inhibitors were considered which affect enzyme activity by direct interaction with the active site. By contrast, allosteric inhibitors modify enzyme activity by binding at sites remote from the catalytic site, thus causing conformational changes (enzymes become inactive). Allosteric inhibition is not considered in the model.

### B.3 Microbial Growth Dynamics – MONOD Kinetics

Microorganisms, mainly bacteria, occur ubiquitously in the subsurface. In groundwater they usually form colonies attached as biofilms on the matrix of porous media or fractured surfaces.

In this Section we establish a link between enzyme kinetics and microbial growth dynamics (population dynamics). At first glance, the expressions of enzyme kinetics and of microbial growth seem to be quite the same. But this is not strictly true. In contrast, we have to deal with two completely different concepts developed at different times and without any reference to each other (see Tab. B.1).

The heart of MONOD’s theory is the concept relating microbial growth rate, μ, with limiting substrate concentration, [S]. The empirical formula MONOD derived in 1942 was

$$(B.17) \quad \mu = \mu_{\text{max}} \frac{[S]}{K_s + [S]} \quad (\text{MONOD equation})$$

with μ<sub>max</sub> as the maximum rate in units of inverse time, T<sup>-1</sup>. It is interesting to note, that originally MONOD did not draw any parallel between his equation and the MICHAELIS-MENTEN equation. The microbial growth rate determines the population dynamics, i.e. the change in biomass or cell density

$$(B.18) \quad \frac{dB}{dt} = (\mu - \Gamma) B$$

where  $B$  is the biomass or cell density and  $\Gamma$  denotes the cell death rate [ $T^{-1}$ ]. Eq. (B.18) is a first-order rate equation. Due to the same mathematical form as in the MICHAELIS-MENTEN equation (hyperbolic form) the MONOD equation implies that  $\mu$  approaches asymptotically the value  $\mu_{\max}$  that remains constant while  $[S]$  increases (similar to the curve in Fig. B.2 at page 63).

**Tab. B.1** Enzyme kinetics vs. population dynamics (basic concepts)

enzyme kinetics	population dynamics
MICHAELIS, MENTEN 1913	MONOD 1942
dynamical variable: substrate $[S]$	biomass or cell density $B$
$-\frac{d[S]}{dt} = v_{\max} \frac{[S]}{K_S + [S]}$ $v_{\max} = k[E_T]$	$\mu = \mu_{\max} \frac{[S]}{K_S + [S]}$ $\frac{dB}{dt} = (\mu - \Gamma) \cdot B$
deduced from well-defined assumptions about the catalytic mechanism	empirical equation

It is a matter of fact that the (total) number of enzymes,  $E_T$ , and the biomass  $B$  are correlated: The greater the biomass the more enzymes are present to degrade the substrate. In a good approximation, enzyme and biomass concentrations should be proportional,  $[E_T] \propto B$ . Both quantities are tied together by the so-called *yield* coefficient  $Y$  (a kind of ‘generalized stoichiometric coefficient’):

$$(B.19) \quad k [E_T] = \frac{\mu_{\max}}{Y} B$$

Using the formulas in Tab. B.1, the dynamics of an ‘*un*isubstrate model’ is described by the following set of differential equations:

$$(B.20) \quad \frac{d[S]}{dt} = -\frac{\mu(t)}{Y} \cdot B(t)$$

$$(B.21) \quad \frac{dB}{dt} = \{ \mu(t) - \Gamma \} \cdot B(t)$$

$$(B.22) \quad \mu(t) = \mu_{\max} \frac{[S]}{K_S + [S]}$$